

AEDC-TR-80-38

C.1

**ARCHIVE COPY
DO NOT LOAN**

Experimental Method for Correcting
Nozzle Aferbody Drag for the
Effects of Jet Temperature



W. L. Peters
ARO, Inc.

July 1981

Final Report for Period October 1978 – August 1980

Approved for public release; distribution unlimited.

Property of U. S. Air Force
AEDC LIBRARY
F40600-81-C-0004

ARNOLD ENGINEERING DEVELOPMENT CENTER
ARNOLD AIR FORCE STATION, TENNESSEE
AIR FORCE SYSTEMS COMMAND
UNITED STATES AIR FORCE



NOTICES

When U. S. Government drawings, specifications, or other data are used for any purpose other than a definitely related Government procurement operation, the Government thereby incurs no responsibility nor any obligation whatsoever, and the fact that the Government may have formulated, furnished, or in any way supplied the said drawings, specifications, or other data, is not to be regarded by implication or otherwise, or in any manner licensing the holder or any other person or corporation, or conveying any rights or permission to manufacture, use, or sell any patented invention that may in any way be related thereto.

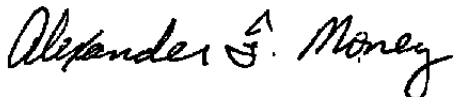
Qualified users may obtain copies of this report from the Defense Technical Information Center.

References to named commercial products in this report are not to be considered in any sense as an indorsement of the product by the United States Air Force or the Government.

This report has been reviewed by the Office of Public Affairs (PA) and is releasable to the National Technical Information Service (NTIS). At NTIS, it will be available to the general public, including foreign nations.

APPROVAL STATEMENT

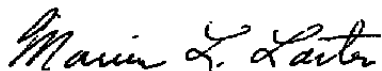
This report has been reviewed and approved.



ALEXANDER F. MONEY
Aeronautical Systems Division
Deputy for Operations

Approved for publication:

FOR THE COMMANDER



MARION L. LASTER
Director of Technology
Deputy for Operations

UNCLASSIFIED

UNCLASSIFIED

20. ABSTRACT (Continued)

(1.0, 1.24, and 2.96) using various unheated jet exhaust gas compositions that allowed a variation in gas constant from 55 to 767 ft-lbf/lbm-°R. Jet mixing effects on afterbody drag coefficient produced by varying jet gas constant and nozzle area ratio at nozzle design pressure ratio, and the drag effects resulting from variations in nozzle pressure ratio at certain overexpanded jet conditions were observed to be similar functions of mass flux ratio. A simple experimental method has been proposed to allow corrections of afterbody drag coefficient data obtained in the wind tunnel (using an ambient temperature air jet) for the effects of jet gas constant. By inference, a similar drag correction can be obtained for the combined effect of gas constant and temperature, assuming their product defines the effects on drag produced by variations in either property.

PREFACE

The work reported herein was conducted by the Arnold Engineering Development Center (AEDC), Air Force Systems Command (AFSC), at the request of the Directorate of Technology (AEDC/DOT). The results were obtained by ARO, Inc., AEDC Group (a Sverdrup Corporation Company), operating contractor for the AEDC, AFSC, Arnold Air Force Station, Tennessee. Testing and analysis of the data were conducted under ARO Project Number P32G-23B. The Air Force project manager for this program was Mr. Elton R. Thompson, DOT. Data analysis was completed on March 23, 1980 and the manuscript was submitted for publication on August 7, 1980.

Mr. W. L. Peters is presently employed by Calspan Field Services, Inc., operating contractor for the Aerospace Flight Dynamics testing effort at the AEDC, AFSC, Arnold Air Force Station, Tennessee.

CONTENTS

	<u>Page</u>
1.0 INTRODUCTION	5
2.0 APPARATUS	
2.1 Test Facility	6
2.2 Test Article and Support System	6
2.3 Gas Supply System	6
2.4 Instrumentation	7
3.0 PROCEDURE	
3.1 Test Conditions and Technique	7
3.2 Data Reduction	8
3.3 Uncertainty of Measurements	9
4.0 RESULTS AND DISCUSSION	
4.1 Jet Exhaust Property Effects	9
4.2 Nozzle Area Ratio Effects	11
4.3 Analysis of Jet Mixing Effects	12
4.4 Proposed Method for Correcting Afterbody Drag for Jet Temperature Effects	14
5.0 CONCLUDING REMARKS	15
REFERENCES	16

ILLUSTRATIONS

Figure

1. Model Dimensions	17
2. Model Installation in Tunnel 1T	18
3. Afterbody and Nozzle Configurations	19
4. Gas Supply System	20
5. Jet Specific Heat Ratio Effects on Afterbody Drag Coefficient Increment	21
6. Nozzle Area Ratio Effects on Afterbody Drag Coefficient Increment	23
7. Effect of Nozzle Area Ratio on Jet Plume Boundaries at Nozzle Design Pressure Ratio ($D_1/D_e = 1.0$)	25
8. Jet Mixing Effects on Afterbody Drag Coefficient Increment Produced by Variations in Jet Molecular Weight and Nozzle Area Ratio	26
9. Typical Variation of Afterbody Drag Coefficient with Nozzle Pressure Ratio	34

<u>Figure</u>	<u>Page</u>
10. Comparison of Jet Mixing Effects on Afterbody Drag Coefficient Increment Produced by Variations in Jet Molecular Weight, Nozzle Area Ratio, and Nozzle Pressure Ratio at Overexpanded Jet Conditions	35
11. Correlation of Jet Mixing Effects on Afterbody Pressure Drag Coefficient Increment as a Logarithmic Function of Jet-to-Free-Stream Mass Flux Ratio	36
12. Proposed Method for Correcting Afterbody Drag for Jet Temperature Effects	39
13. Comparisons of Actual and Estimated Drag Coefficient Sensitivity to the $R_j T_{t_j}$ Product	40

TABLES

1. External Pressure Orifice Locations	43
2. Test Summary	44
NOMENCLATURE	45

1.0 INTRODUCTION

Wind tunnel tests with subscale models frequently use an ambient-temperature high pressure air jet to simulate the hot engine jet exhaust. Several experimental investigations (Refs. 1 and 2) have shown that jet temperature can directly affect nozzle afterbody drag, and thus, must be either duplicated or corrected for if afterbody drag performance is to be accurately defined. One study (Ref. 3) has examined the prospects of simulating these temperature effects by altering the chemical composition of the jet exhaust. In Ref. 3, the effects of jet specific heat ratio, γ_j (a secondary temperature effect) and the effects of jet molecular weight on afterbody drag were evaluated separately in an effort to understand the physical mechanisms and associated jet parameters. Because of the frequency with which the $R_j T_{tj}$ product occurs in many flow parameters, variations in jet molecular weight (or gas constant, R_j) were chosen to simulate variations in the jet total temperature, T_{tj} . It was concluded that variations in specific heat ratio affect drag primarily through changes in the inviscid plume shape and that gas constant (or molecular weight) and by inference, temperature, influence drag through processes normally associated with jet entrainment of the free-stream flow. No jet simulation parameter correlating mixing effects was isolated; however, several parameters were found which could provide the basis for the adjustment of jet molecular weight to give the proper simulation of a hot jet in wind tunnel experiments.

The current investigation was conducted to analyze further jet mixing effects on afterbody drag by coupling variations in jet molecular weight with changes in nozzle exit area to throat area ratio, A_e/A^* . The nozzle area ratio effects on afterbody drag coefficient were not completely defined when traditional inviscid jet plume shape parameters such as maximum plume to nozzle exit diameter ratio were matched in an experimental study reported in Ref. 4. These experimental differences in drag coefficient were attributed to jet mixing effects and thus were similar to the effects of jet molecular weight. The present experiments were designed to choose area ratio and jet molecular weight values selectively to allow flow parameters, such as velocity, density, mass flow, and kinetic energy, to be individually held constant in an attempt to isolate those parameters which define the jet mixing effects. The objective was to apply this information to determine a practical method to correct for or simulate the effects of jet temperature on afterbody drag in wind tunnel experiments.

Experiments using a strut-supported pod model representing a separated (25-deg boat-tail) afterbody contour were conducted in Tunnel 1T. Integrated afterbody pressure drag coefficient data were acquired for three nozzle area ratios (1.0, 1.24, and 2.96) using various jet exhaust gas compositions which allowed a variation in gas constant, R_j from 55 to 767 ft-lbf/lbm-°R and a variation in specific heat ratio from 1.40 to 1.66. These gases were

composed of either nitrogen (N_2), hydrogen (H_2), helium (He), or various mixtures of N_2 and H_2 . Exhaust gas total temperature was maintained at approximately 630°R. Testing was conducted at nominal free-stream Mach numbers ranging from 0.6 to 1.2, at model nozzle total pressure ratios from approximately 1 to 32, and a model angle of attack of 0 deg.

2.0 APPARATUS

2.1 TEST FACILITY

Tunnel 1T is a continuous-flow, nonreturn wind tunnel capable of being operated at Mach numbers from 0.2 to 1.5, using variable nozzle contours above $M_\infty = 1.10$. The tunnel is operated in a stilling chamber total pressure about 2,850 psfa with a ± 5 percent variation, dependent on tunnel resistance and ambient atmospheric conditions. The total temperature can be varied from 80 to 120°F above ambient temperature as necessary to prevent visible condensation in the test section. The test section is 1-ft square and 37.5 in. long with 6 percent porous perforated walls. A detailed description of the tunnel and its operating capabilities is given in Ref. 5.

2.2 TEST ARTICLE AND SUPPORT SYSTEM

The experimental data for this investigation were acquired from tests conducted with a strut-mounted axisymmetric model with a 25-deg boattail. This model, more fully described in Ref. 3 and shown in Figs. 1 and 2, was modified to accommodate any one of three internal nozzle inserts with the same exit diameter but different throat diameters. The nozzle inserts represented nozzle exit area to throat area ratios of 1.0, 1.24, and 2.96 and are shown in Fig. 3, along with the external afterbody contour dimensions for the model.

2.3 GAS SUPPLY SYSTEM

Tests were conducted using jet exhaust gases composed of either pure N_2 , H_2 , or He, and differing mixtures by weight of N_2 and H_2 . A gas piping system, shown in Fig. 4 and located externally to the wind tunnel, controlled, temperature-conditioned, and supplied the various gases to the model. An appropriate choked venturi metering section was used for measurement of the mass flow. Each gas was ducted through a double-tube heat exchanger for temperature conditioning and was supplied to a manifold connected to the base of the model support strut. For a jet exhaust composed of a mixture of N_2 and H_2 gases, the two gas flows were merged before they entered the heat exchanger.

2.4 INSTRUMENTATION

The model was instrumented with 19 static pressure orifices distributed axially and circumferentially about the afterbody external surface. In addition, the model had three nozzle base pressure orifices at three circumferential locations. The orifice positions are presented in Table 1. The pressures were measured by the Tunnel 1T pressure system comprised of a five-module 48-port Scanivalve®. Each module had a 15-psid differential transducer, and a transducer calibration constant was determined for every data point. The model also incorporated four static pressures within the plenum chamber located upstream of the nozzle insert which were measured by one 200-psia and three 500-psia strain-gage transducers. Two copper-constantan thermocouples were located in the gas piping system, in front of the model strut. The temperature and model plenum pressure measurements were used for isentropic computations of nozzle mass flow as a check on the venturi measurements.

Gas supply system instrumentation (shown in Fig. 4) consisted of upstream venturi and throat static pressures measured by strain-gage transducers (with a range of 2,000 psia) and two upstream venturi temperatures measured by copper-constantan thermocouples. These measurements were used to compute mass flow through the venturi metering sections. All electrical signals from instrumentation data channels were processed through an analog-to-digital converter, recorded on paper tape, and fed to a facility computer for on-line data reduction.

3.0 PROCEDURE

3.1 TEST CONDITIONS AND TECHNIQUE

Test data were acquired at free-stream Mach numbers of 0.6, 0.9, and 1.2 as shown by the test summary in Table 2. A test section wall angle of 0 deg was maintained at all test conditions, and testing was conducted only at an angle of attack of 0 deg. Nozzle total pressure ratio was the primary run variable, ranging from approximately 1 to 32 depending on gas supply pressure, nozzle area ratio, and free-stream Mach number.

The data acquisition procedure consisted of setting the appropriate free-stream conditions, regulating the nozzle plenum chamber static pressure and/or venturi supply pressure(s) to give the required nozzle total pressure ratio, and adjusting the steam heater flow to produce a desired gas supply temperature in the plenum chamber. A plenum chamber temperature of approximately 630°R (± 30) was maintained to correspond closely to the free-stream total temperature.

3.2 DATA REDUCTION

The primary parameter used to assess the effects of changes in the jet is the integrated afterbody pressure drag coefficient. This parameter is based on a maximum model cross-sectional area of approximately 0.76 sq. in. and was determined by numerically integrating the pressure distribution on the afterbody surface, excluding the nozzle base area. The drag coefficient represented the pressure drag on the afterbody aft of Model Station 14.068.

Venturi mass flow was calculated from

$$\dot{m}_v = \frac{P_{t_v} D_v^{*2} \left[\gamma_v \left(\frac{2}{\gamma_v + 1} \right)^{(\gamma_v + 1)/(\gamma_v - 1)} \right]^{\frac{1}{\gamma}} K_v K_D}{\left(R_v T_{t_v} \right)^{\frac{1}{\gamma}}} \quad (1)$$

where K_v is a constant (a function of π and g), K_D is the discharge coefficient at the venturi throat assuming laminar flow, P_{t_v} and T_{t_v} are the respective total pressure and temperature measured upstream of the venturi, and D_v^* is the venturi throat diameter. The static pressure was measured upstream of the venturi rather than the total pressure, but because of the large contraction area ratio, it was assumed equivalent for mass flow computations. The ratio of specific heats used for venturi computations for N_2 and H_2 gases was determined from the upstream venturi static pressure and temperature using real gas properties. Real gas data for N_2 and H_2 were obtained from Refs. 6 and 7, respectively. Mass flow computations for He gas used a value of 1.659 for the specific heat ratio.

Isentropic relations were used for computation of all nozzle flow and jet parameters presented herein. An average model plenum chamber static pressure and the nozzle contraction area ratio were used to calculate the nozzle total pressure. The nozzle ratio of specific heats, γ_j was assumed to be a constant value of 1.40 (calorically perfect) for jet exhausts composed of N_2 , H_2 , or any mixture thereof, and 1.659 for a jet exhaust composed of He.

The gas constant, R_j for a nozzle flow composed of a mixture of N_2 and H_2 gases was computed from

$$R_{\text{mixture}} = \frac{\left(\dot{m}_{v_{N_2}} \right) \left(R_{N_2} \right) + \left(\dot{m}_{v_{H_2}} \right) \left(R_{H_2} \right)}{\dot{m}_{v_{N_2}} + \dot{m}_{v_{H_2}}} \quad (2)$$

3.3 UNCERTAINTY OF MEASUREMENTS

Uncertainties in the instrumentation systems were estimated from repeat calibration of the systems against secondary standards whose uncertainties are traceable to the National Bureau of Standards calibration equipment. The tunnel parameter and instrument uncertainties are combined using the Taylor series method of error propagation described in Ref. 8 to determine the uncertainties of the reduced parameters. The uncertainties for a 95-percent confidence level are

<u>Parameter</u>	<u>Value</u>	<u>Uncertainty</u>
M_∞	0.9	± 0.0037
q_∞, psf	953.1	± 0.0258
C_{p_x}	-0.1696	± 0.0070
NPR	4.397	± 0.1032
$R_j, \text{ft-lbf/lbm}^{-0.5}$	411.4	± 3.89
C_{D_p}	0.1380	± 0.0028

Since increments rather than absolute values of afterbody drag coefficient, C_{D_p} , are of primary interest for the evaluation of jet mixing effects, the repeatability instead of the computed uncertainty gives a realistic measure of data reliability. Sufficient jet-off data were available from the present investigation to statistically determine the repeatability of C_{D_p} since jet-off drag is not a function of nozzle internal geometry. An estimate of repeatability at a 95-percent confidence level for C_{D_p} using 39 samples of jet-off drag coefficient ($C_{D_p} \approx 0.1378$) obtained at $M_\infty = 0.9$ is ± 0.0030 (which is approximately equivalent to ± 0.0003 if C_{D_p} is based on typical aircraft wing area).

4.0 RESULTS AND DISCUSSION

Although some data are presented at free-stream Mach numbers 0.6 and 1.2, data presented herein are primarily for a Mach number 0.9 since, in general, jet temperature effects have been found to be similar at all subsonic and supersonic Mach numbers (Refs. 1 and 2). The jet effects shown are presented primarily as an afterbody drag coefficient increment obtained by subtracting the jet-off drag coefficient from the jet-on drag coefficient.

4.1 JET EXHAUST PROPERTY EFFECTS

The parameter NPR is commonly used in nozzle afterbody testing as the jet simulation parameter for correlating afterbody drag. Afterbody drag coefficient data from Ref. 1

demonstrate a significantly higher drag coefficient is obtained when a cold, high-pressure air jet is used in a wind tunnel model to represent the hot exhaust jet of a full-scale aircraft.

The effects of jet specific heat ratio, γ_j on drag coefficient were reported in Ref. 3, where values of γ_j corresponding to a cold air jet and to a heated exhaust, representative of a turbojet or turbofan exhaust, were investigated. The variation in γ_j was obtained by using cold ethylene and nitrogen as jet exhaust gases. The data from Ref. 3 indicated that afterbody drag coefficient is not affected by variations in γ_j if the data were presented as functions of any one of several inviscid jet plume shape parameters such as D_1/D_e shown in Fig. 5a. The parameter D_1/D_e represents the plume maximum diameter determined from isentropic relationships normalized by nozzle exit diameter.

In Fig. 5b incremental drag coefficient data from current wind tunnel experiments are presented at free-stream Mach numbers 0.6, 0.9, and 1.2 for γ_j of 1.40 and 1.66. The variation of γ_j shown in Fig. 5b was accomplished using helium and a nitrogen-hydrogen mixture as jet exhaust gases at fixed temperature. In general, the correlation of drag coefficient data from present experiments as a function of D_1/D_e (or any other inviscid jet plume shape parameter) is not as good as that reported in Ref. 3. At Mach number 1.2, a downward shift in drag coefficient is obtained as γ_j is increased from 1.40 to 1.66. Contradictory results are shown at a free-stream Mach number 0.9, where the variation in drag coefficient data with γ_j is not consistent over the range of D_1/D_e . The poorer correlation of γ_j effects in current experiments compared to those from Ref. 3 suggests that matching a plume shape parameter does not always fully compensate for the effects of γ_j on drag. However, the data uncertainty (approximately ± 30 drag counts at Mach number 0.9) could account for the drag differences shown in Fig. 5b.

Effects similar to those obtained when varying T_{ij} are obtained when jet molecular weight represented by gas constant (R_j) is varied (Ref. 3).

A near-constant reduction of the drag coefficient occurs over the range of D_1/D_e when R_j or T_{ij} is increased. The mixing effects produced by either of these jet properties appear nearly independent of inviscid effects.

Since the product of R_j and T_{ij} occurs in the equations relating many flow parameters which have some relationship to the viscous mixing effects of the jet, it is hypothesized that changes in the $R_j T_{ij}$ product caused by varying either R_j or T_{ij} will result in similar effects on drag, provided the inviscid jet plume shape remains constant. Further experiments are planned to determine the relationship of jet mixing effects on afterbody drag produced by independent variations in these two jet properties. However, for subsequent discussion, the

$R_j T_{tj}$ product will be used the implication that either R_j or T_{tj} is the correct correlating variable.

4.1.1 Hot Jet Simulation

Several possible methods of simulation of a hot jet with an ambient temperature jet or correction of drag data for the effect of jet temperature are suggested from these results. The methods, all of which first require matching an inviscid jet plume shape parameter (such as D_1/D_e), are as follows:

1. Simulation of the desired temperature effect by using a mixture of gases having the desired $R_j T_{tj}$ product.
2. Testing with several gases, determining the configuration drag sensitivity to $R_j T_{tj}$, and applying corrections to data obtained with ambient temperature air.
3. Alteration of jet conditions, other than by varying R_j or T_{tj} , to effectively simulate jet conditions at an elevated jet temperature. It is suggested specifically that by varying nozzle area ratio (A_e/A^*), parameters (such as velocity, density, etc.) can be varied that should be related to jet mixing while simultaneously matching D_1/D_e .

Of the three methods, the latter represents the simplest method of varying "mixing parameters" because it allows the use of an ambient temperature air jet exhaust in conventional nozzle afterbody tests. The present experiments were conducted to compare the effects associated with varying $R_j T_{tj}$ and A_e/A^* .

4.2 NOZZLE AREA RATIO EFFECTS

The effects of A_e/A^* on incremental afterbody drag coefficient are shown in Fig. 6 for the 25-deg boattail at free-stream Mach numbers 0.6, 0.9, and 1.2. The data were obtained with γ_j , R_j , and T_{tj} constant. The drag coefficient differences obtained with the various area ratio nozzles are not the same functional family as a function of the shape parameter, D_1/D_e . The large variation of the data obtained with the $A_e/A^* = 1.0$ nozzle compared to the data obtained with the other nozzles is believed to be caused by both jet mixing and jet plume shape differences caused, in turn, by changes in the axial location of the plume maximum diameter. Only near the nozzle design condition ($D_1/D_e = 1$) is there a consistent variation in the drag coefficient increment with nozzle area ratio. At this condition an increase in nozzle area ratio results in an increase in drag coefficient increment. Since the inviscid jet plume shape is nearly cylindrical at $D_1/D_e = 1$, differences in drag coefficient

variation with A_e/A^* nozzles should be primarily a result of jet mixing. Jet plume shape boundaries computed by the method of characteristics (MOC) assuming quiescent free-stream conditions are shown in Fig. 7 to illustrate the similarities in plume shape at nozzle design pressure ratio for various nozzle area ratios. Thus, subsequent discussion of mixing effects on afterbody drag produced by variations in area ratio and gas constant will be restricted to nozzle design pressure ratios.

4.3 ANALYSIS OF JET MIXING EFFECTS

The combined effects of varying A_e/A^* and R_j on the incremental afterbody drag coefficient at the nozzle design pressure ratio (approximately cylindrical inviscid plume shape) for the 25-deg boattail are presented in Fig. 8. The data are presented as a function of several flow parameters that are related as functions of R_j , T_{tj} , and/or A_e/A^* . The parameters, velocity ratio (V_e/V_∞), density ratio (ρ_e/ρ_∞), momentum ratio ($\rho_e V_e^2/\rho_\infty V_\infty^2$), kinetic energy ratio ($\rho_e V_e^3/\rho_\infty V_\infty^3$), and the induced velocity ratio ($\bar{\phi}$) provide little or no correlation of the data. In Fig. 8d, ΔC_{D_p} does not vary linearly with $V_e V_\infty$ (which is proportional to $\sqrt{R_j}$). This contradicts statements in Ref. 3 based on only a limited amount of data implying a linear relationship between afterbody drag and $\sqrt{R_j}$. Of the parameters used, only mass flux ratio, $\rho_e V_e / \rho_\infty V_\infty$ (Fig. 8e) provides a reasonable correlation of the drag coefficient increments produced by varying R_j and A_e/A^* . This parameter was suggested in Ref. 9 as a possible simulation parameter for the effects of jet entrainment.

The drag coefficient increment, ΔC_{D_p} , has a nearly linear variation with the $R_j T_{tj}$ product (Fig. 8a) and the induced velocity ratio, $\bar{\phi}$ (Fig. 8h) as R_j is varied at a constant A_e/A^* . Reference 10 indicates that $\bar{\phi}$, a turbulent mixing parameter, is a strong function of the $R_j T_{tj}$ product, which explains why the drag variation is similar as a function of either parameter.

As A_e/A^* is varied at a constant $R_j T_{tj}$, the drag coefficient ΔC_{D_p} also has a linear variation with jet exit Mach number, M_e , (Fig. 8b) and jet-to-free-stream momentum ratio, $\rho_e V_e^2 / \rho_\infty V_\infty^2$ (Fig. 8f). The limited amount of area ratio variation does not clearly indicate which parameter, M_e or $\rho_e V_e^2 / \rho_\infty V_\infty^2$ (which is proportional to M_e^2), if either, is the true linear variable.

Assuming linearity with the parameters, $R_j T_{tj}$ and M_e , the slopes $\delta \Delta C_{D_p} / \delta (R_j T_{tj})$ and $\delta \Delta C_{D_p} / \delta M_e$ can be selected to be independent of M_e and $R_j T_{tj}$, respectively. With additional assumptions that $\Delta C_{D_p} = f(R_j, T_{tj}, M_e)$ at constant jet plume shape ($D_1/D_e = \text{constant}$) an equation for ΔC_{D_p} can be written as independent functions of $R_j T_{tj}$ and M_e that defines ΔC_{D_p} for the test conditions shown. This equation would have the following form:

$$\Delta C_{D_p} = \Delta C_{D_p \text{REF}} + \frac{\delta \Delta C_{D_p}}{\delta (R_j T_{t_j})} \left(R_j T_{t_j} - R_j T_{t_j \text{REF}} \right) + \frac{\delta \Delta C_{D_p}}{\delta M_e} \left(M_e - M_{e \text{REF}} \right) \quad (3)$$

where $\delta \Delta C_{D_p}/\delta(R_j T_{t_j})$ is the average slope of the data from Fig. 8a, $\delta \Delta C_{D_p}/\delta M_e$ is the average slope of the data from Fig. 8b, and $\Delta C_{D_p \text{REF}}$, $(R_j T_{t_j})_{\text{REF}}$, and $M_{e \text{REF}}$ are data values at a specified test condition. (A similar equation could be written by replacing $R_j T_{t_j}$ by \bar{f} and M_e by $\rho_e V_e^2 / \rho_\infty V_\infty^2$.)

In practice, $\delta \Delta C_{D_p}/\delta M_e$ can be determined experimentally in the wind tunnel by varying A_e/A^* and using a jet exhaust composed of cold air. If the relationship between $\delta \Delta C_{D_p}/\delta M_e$ and $\delta \Delta C_{D_p}/\delta(R_j T_{t_j})$ were known, then data obtained by varying area ratio in the wind tunnel could be used to predict $\delta \Delta C_{D_p}/\delta(R_j T_{t_j})$ and thereby correct for the effects of varying $R_j T_{t_j}$. It has been shown (Fig. 8e) that the effects of A_e/A^* and $R_j T_{t_j}$ on afterbody drag can be correlated by the mass flux parameter, $\rho_e V_e / \rho_\infty V_\infty$, and thus can be used as a basis for relating the drag sensitivity to the two parameters. Subsequent discussion provides an alternate experimental method, which is easier than varying A_e/A^* , to estimate the effects of $R_j T_{t_j}$ on drag by using a jet composed of cold air and $\rho_e V_e / \rho_\infty V_\infty$ as a correlation parameter.

A typical variation of afterbody drag coefficient as a function of nozzle pressure ratio, NPR, is shown in Fig. 9. References 2 and 11 postulate that increasing entrainment tends to accelerate the flow over the afterbody, thereby resulting in a decrease in afterbody surface pressure and an increase in drag coefficient. It is hypothesized that in the region between the "drag bucket" and the "peak drag" at overexpanded jet conditions (Fig. 9), that afterbody drag is increasing as a result of increasing jet entrainment. If jet mixing is the mechanism acting to increase drag in this overexpanded jet regime and if the parameter $\rho_e V_e / \rho_\infty V_\infty$ is the correct mixing parameter, drag coefficient data obtained by either varying $R_j T_{t_j}$, A_e/A^* , or NPR at the overexpanded jet conditions (where entrainment is important) should correlate by matching $\rho_e V_e / \rho_\infty V_\infty$. It should be noted that the "peak drag" point in Fig. 9 sometimes occurs at nozzle pressure ratios less than nozzle design pressure ratio, depending upon nozzle external geometry and free-stream Mach number.

In Fig. 10, a comparison of drag coefficient increments obtained with variations in R_j and A_e/A^* at nozzle design pressure ratio and variations in NPR at overexpanded jet conditions are shown as a function of $\rho_e V_e / \rho_\infty V_\infty$. Only data obtained at conditions below or equal to design nozzle pressure ratio where entrainment effects are dominant are used. In general, an approximate correlation of the R_j , A_e/A^* , and NPR (overexpanded) effects on drag coefficient increment are obtained as a function of $\rho_e V_e / \rho_\infty V_\infty$ which implies that the same physical mechanism causes changes in drag by varying these three parameters.

In Fig. 11, incremental afterbody drag coefficient data illustrate that effects produced by varying $R_j A_e / A^*$, and NPR at overexpanded jet conditions are linearly correlated as a function of the logarithm of $\rho_e V_e / \rho_\infty V_\infty$. In general, the range of the drag coefficient data is approximately three to eight times greater than the data scatter shown, depending upon free-stream Mach number. The best data correlation is obtained at $M_\infty = 1.2$ where mixing effects appear to produce the largest effects on afterbody drag.

4.4 PROPOSED METHOD FOR CORRECTING AFTERBODY DRAG FOR JET TEMPERATURE EFFECTS

In earlier discussion, it was suggested that the effects of varying $R_j T_{tj}$ might be simulated by altering jet conditions in some other manner. The drag correlation in Fig. 10 indicates this can be accomplished by varying either nozzle area ratio or nozzle pressure ratio at overexpanded jet conditions to vary jet mass flux. As shown by the solid symbols in Fig. 10, a significant portion of the data can be obtained in wind tunnel experiments using a jet composed of cold air. A majority of these data were obtained with NPR as a variable at overexpanded jet conditions. For typical nozzle afterbody wind tunnel tests, the data can be obtained easier by varying NPR than by varying nozzle area ratio because a change in nozzle area normally requires a model change. The data at overexpanded jet conditions can be normally obtained in the wind tunnel at the same time "C_{Dp} versus NPR" data are obtained to match various flight conditions and thus are preferred to predict drag effects resulting from changes in $R_j T_{tj}$.

A method is outlined in Fig. 12 which demonstrates how afterbody drag coefficient data from the wind tunnel using an air jet exhaust might be used to estimate the effects of T_{tj} on drag. The method involves two corrections to drag representing jet mixing effects (R_j or T_{tj} effect) and jet plume shape effects (γ_j effect).

An estimate of jet mixing effects is obtained by using data from the entrainment-dominated region between the "drag bucket" and the nozzle design pressure ratio (Fig. 9). These drag data are assumed to approximate data with $R_j T_{tj}$ as a variable when presented as a function of jet mass flow. Earlier discussions have indicated that the drag sensitivity to the $R_j T_{tj}$ product is essentially linear. By using the measured jet mass flow, \dot{m}_j , an equivalent $R_j T_{tj}$ product for the data at overexpanded jet conditions can be calculated assuming M_e and P_e equal to the nozzle design values by

$$(R_j T_{tj})_{EQ} = \frac{\gamma_j g \left(1 + \frac{\gamma_j - 1}{2} M_e^2 \right) P_e^2 M_e^2 A_e^2}{\dot{m}_j^2} \quad (4)$$

Equation (4) is based on the continuity equation assuming isentropic flow. Measured drag coefficient values and associated values of $(R_j T_{ij})_{EQ}$ for the data at overexpanded jet conditions can be used to obtain the slope of ΔC_{D_p} versus $(R_j T_{ij})_{EQ}$ by the linear least-squares method; the slope can then be used in Eq. (3) to determine the effects of either increasing or decreasing $R_j T_{ij}$ on drag coefficient. This slope can also be used to correct incremental drag coefficient data for mixing effects at fixed jet plume shape conditions at nozzle pressure ratios greater than the design value ($D_1/D_e > 1$) since, from Ref. 3, the effects of R_j and T_{ij} on the slope are independent of inviscid jet plume shape.

In Fig. 13, an estimate of the drag coefficient variation with the $R_j T_{ij}$ product using data at the overexpanded jet conditions (with NPR variable) and Eq. (4), is compared to actual drag data obtained with R_j varied at nozzle design pressure ratio. The data from Ref. 3 are shown for both 15-deg and 25-deg boattail geometries at free-stream Mach numbers 0.6, 0.9, and 1.2. The data at overexpanded jet conditions were obtained using a nitrogen jet. The slopes of both the actual and estimated curves agree well. As a result it is concluded that data obtained at the overexpanded jet conditions from typical wind tunnel tests can be used to determine the drag sensitivity to R_j and therefore, by inference, the sensitivity to $R_j T_{ij}$.

5.0 CONCLUDING REMARKS

The objective of this investigation was to determine a method of correcting, simulating, or compensating for the mixing effects of jet temperature on afterbody drag coefficient. Data for this investigation were obtained from experiments conducted using a strut-mounted model with a 25-deg boattail and three nozzle internal geometries having nozzle area ratios of 1.0, 1.24, and 2.96, respectively. Essentially unheated gases representing different jet compositions were used to separately vary the exhaust gas constant from 55 to 767 ft-lbf/lbm-°R and the exhaust ratio of specific heats from 1.40 to 1.66.

The significant results and conclusions obtained in this evaluation of combined effects of jet exhaust properties and nozzle area ratio on afterbody drag coefficient are:

1. A simple experimental method has been devised for correcting afterbody drag coefficient data obtained in the wind tunnel (using cold air jet) for the effects of gas constant, R_j . By inference, a similar drag correction can be obtained for the combined effect of R_j and T_{ij} assuming the $R_j T_{ij}$ product relates drag effects produced by variations in either of these properties.
2. Effects on afterbody incremental drag coefficient produced by varying jet gas constant (R_j) and nozzle area ratio (A_e/A^*) at nozzle design pressure ratio, and from variations in NPR at certain overexpanded jet conditions are similar functions of mass flux ratio ($\rho_e V_e / \rho_\infty V_\infty$).

3. Afterbody incremental drag coefficient at a fixed inviscid jet plume shape linearly decreases with increasing R_j (or by inference $R_j T_{l_j}$ product) and the slope is independent of A_e/A^* and inviscid jet plume shape.
4. At nozzle design pressure ratio, afterbody incremental drag coefficient increases linearly with increasing jet exit Mach number, M_e , and the slope is independent of R_j (or by inference the $R_j T_{l_j}$ product).

REFERENCES

1. Peters, W. L. "An Evaluation of Jet Simulation Parameters for Nozzle Afterbody Testing at Transonic Mach Numbers." AEDC-TR-76-109 (ADA031525), October 1976.
2. Compton, W. B. "Effects of Jet Exhaust Gas Properties on Exhaust Simulation and Afterbody Drag." NASA TR R-444, October 1975.
3. Peters, W. L. "Jet Simulation Techniques: Simulation of Temperature Effects by Altering Gas Composition." AEDC-TR-78-43 (ADA067084), March 1979.
4. Price, Earl A. "A Parametric Investigation of the Annular Jet Concept for Obtaining Afterbody Drag at Transonic Mach Numbers." AEDC-TR-77-104 (ADA050891), February 1978.
5. *Test Facilities Handbook* (Eleventh Edition). "Propulsion Wind Tunnel Facility, Vol. 4." Arnold Engineering Development Center, June 1979.
6. Hilsenrath, Joseph, et al. "Tables of Thermal Properties of Gases." National Bureau of Standards, Circular 564, November 1, 1955.
7. Johnson, Robert C. "Real Gas Effects in Critical Flow-Through Nozzles and Tabulated Thermodynamic Properties." NASA TN D-2565, January 1965.
8. Abernethy, R. B. and Thompson, J. W., Jr. "Handbook - Uncertainty in Gas Turbine Measurements." AEDC-TR-73-5 (AD755356), February 1973.
9. Pindzola, M. "Jet Simulation in Ground Test Facilities." AGARDograph 79, November 1963.
10. Bauer, R. C. "A Method for Estimating Jet Entrainment Effects on Nozzle-Afterbody Drag." AEDC-TR-79-85 (ADA080955), February 1980.
11. Bergman, Dave. "Effects of Engine Exhaust Flow on Boattail Drag." *J. Aircraft*, Vol. 8, No. 6, June 1971, pp. 434-439.

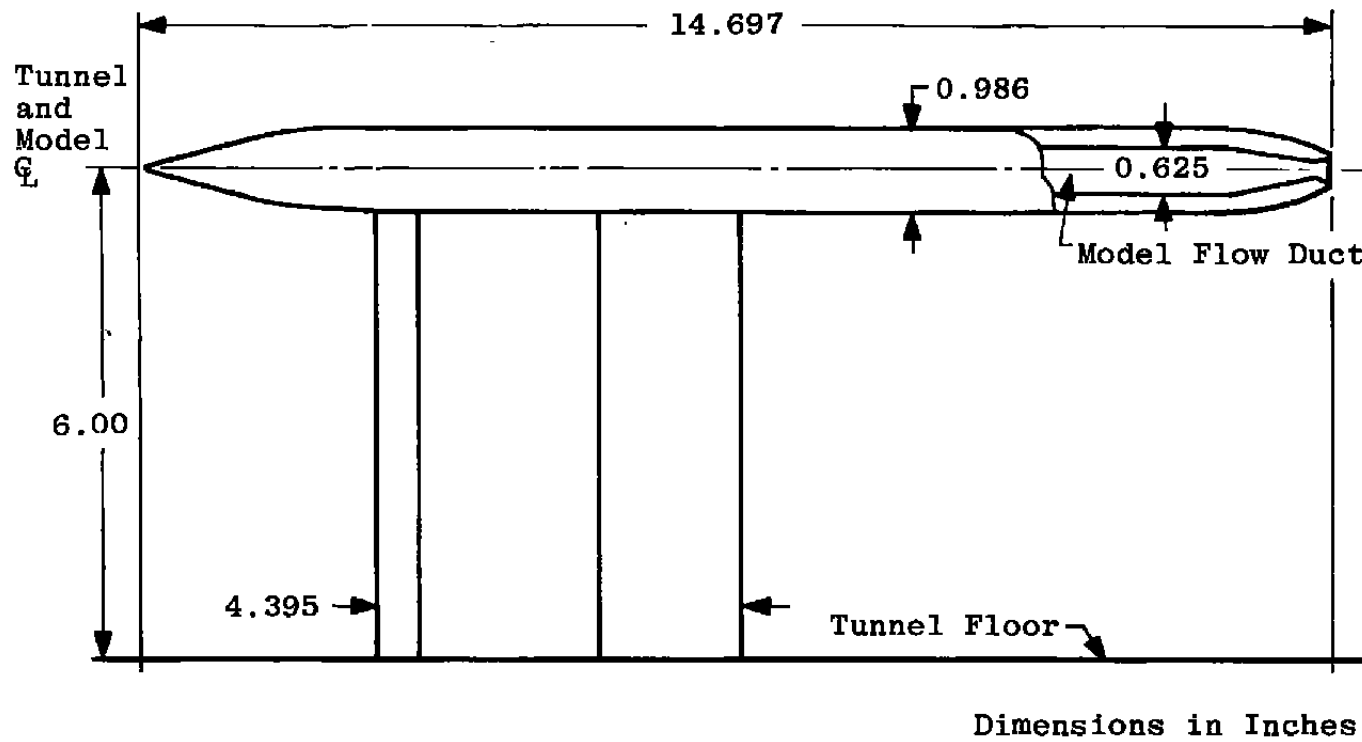


Figure 1. Model dimensions.

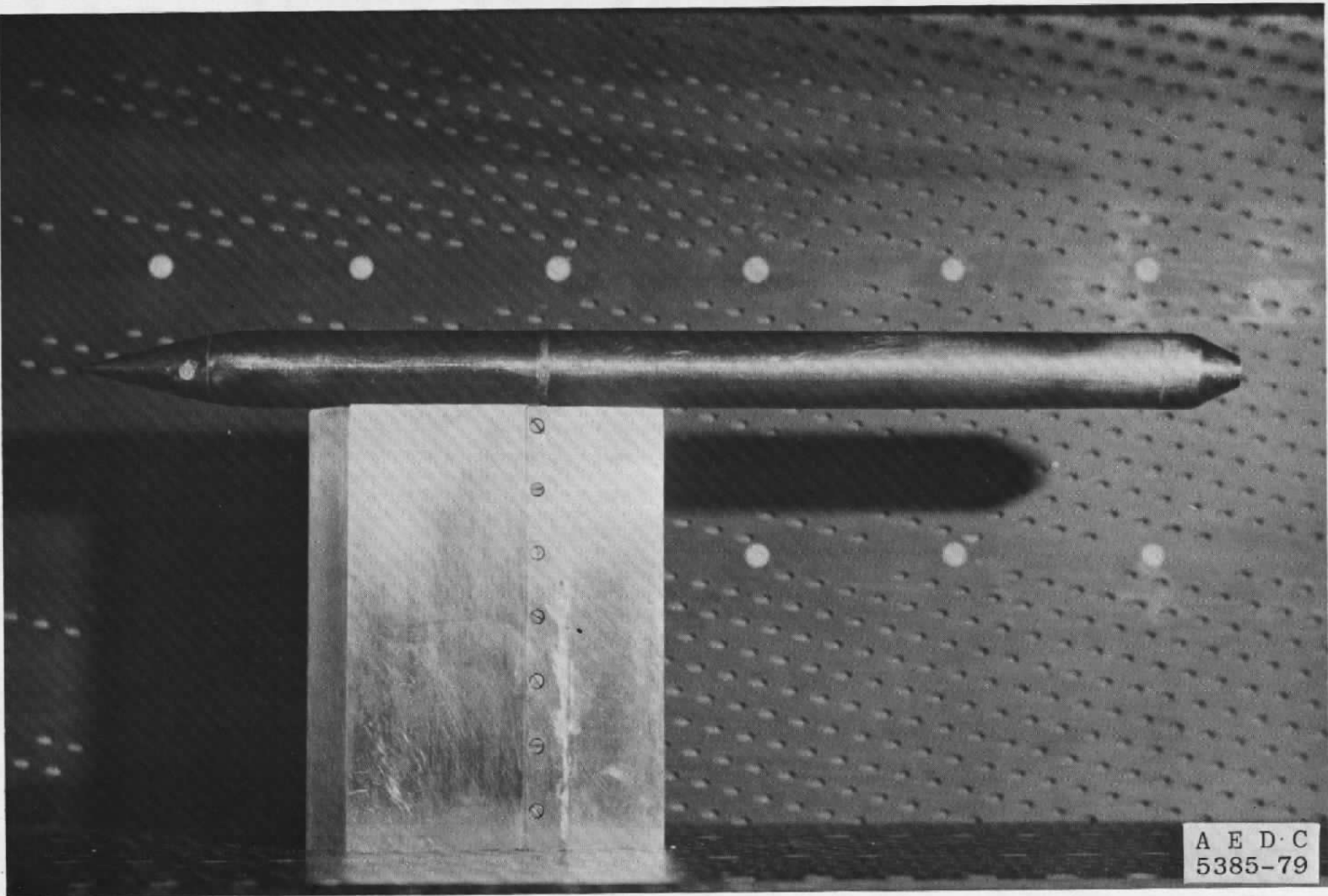
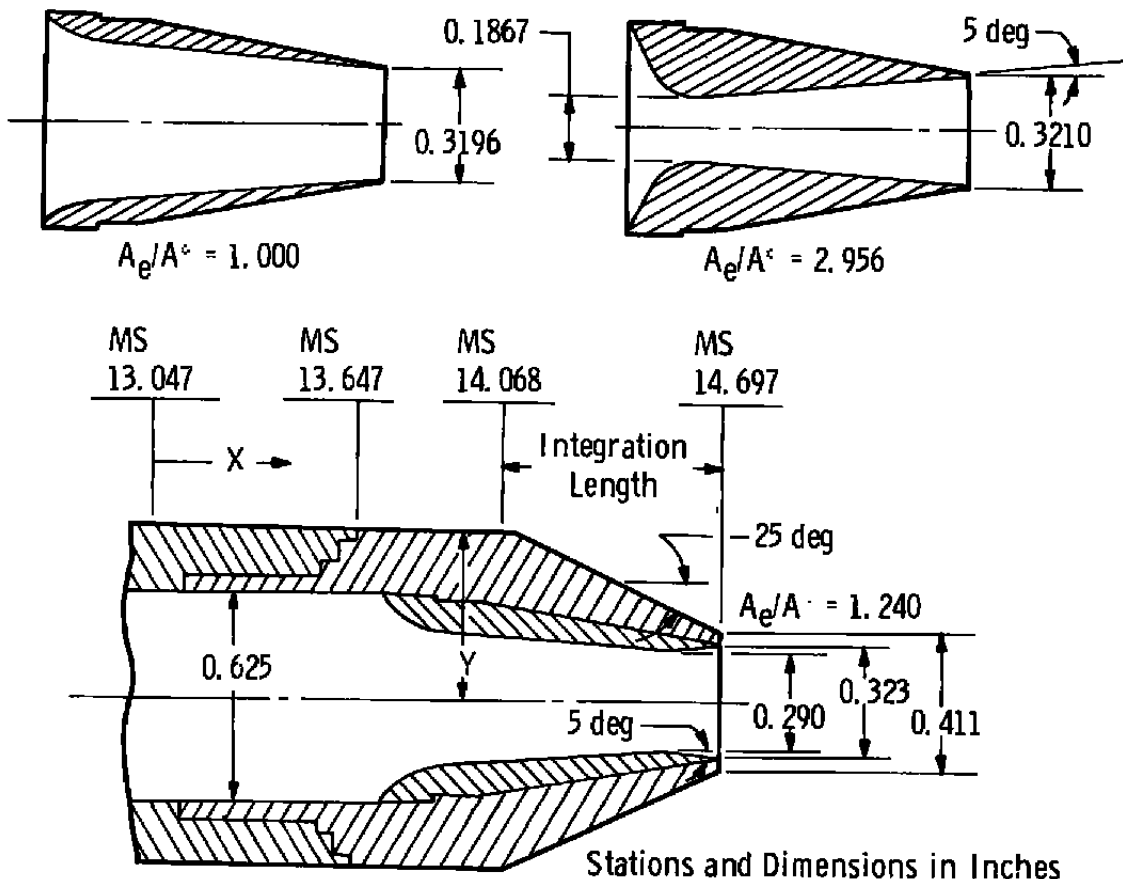


Figure 2. Model installation in Tunnel 1T.



X	Y	X	Y
1.021	0.492	1.305	0.368
1.034	0.491	1.354	0.344
1.058	0.487	1.403	0.322
1.083	0.479	1.453	0.299
1.108	0.468	1.502	0.276
1.157	0.444	1.552	0.252
1.206	0.419	1.601	0.230
1.256	0.393	1.650	0.205

Figure 3. Afterbody and nozzle configurations.

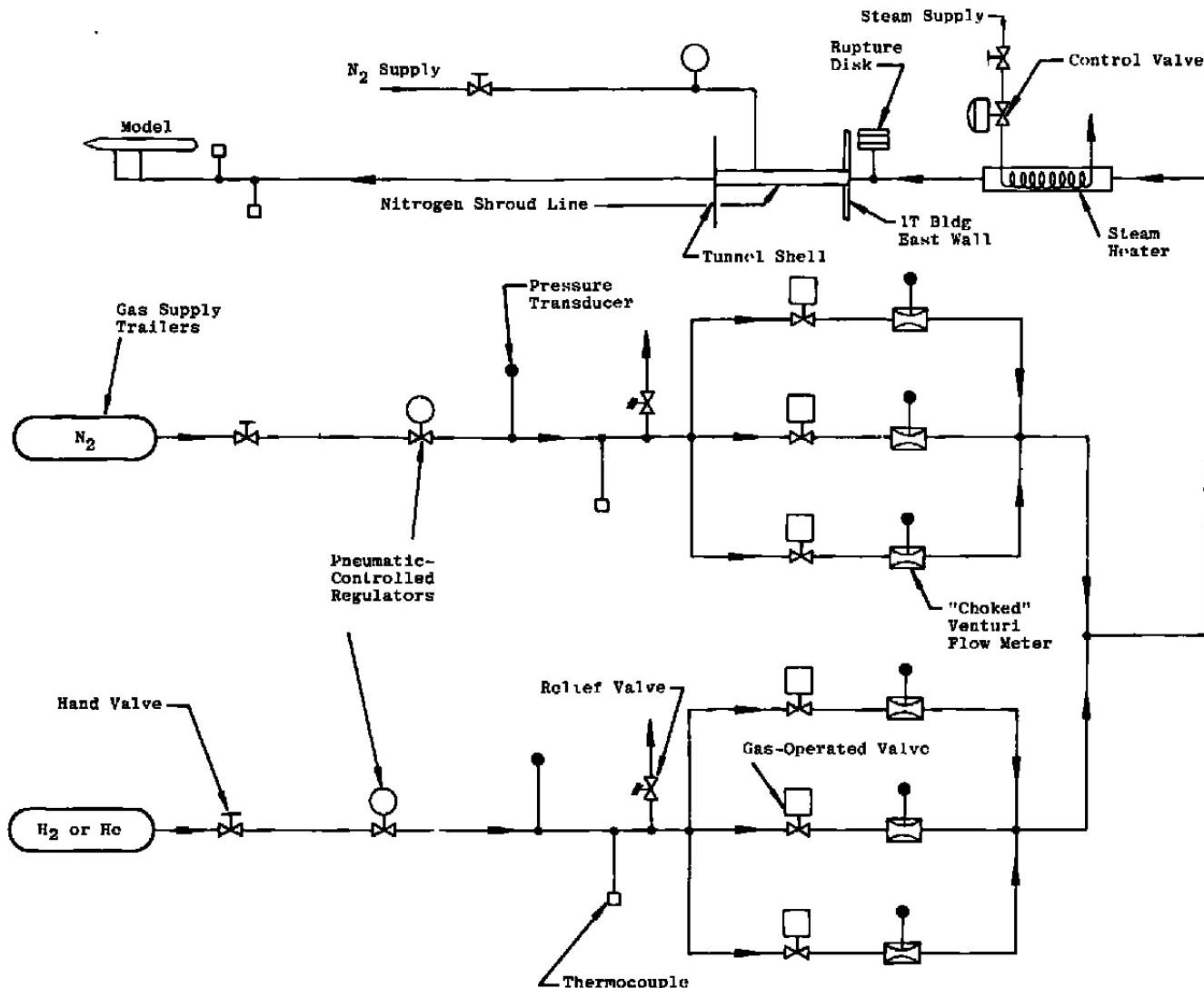
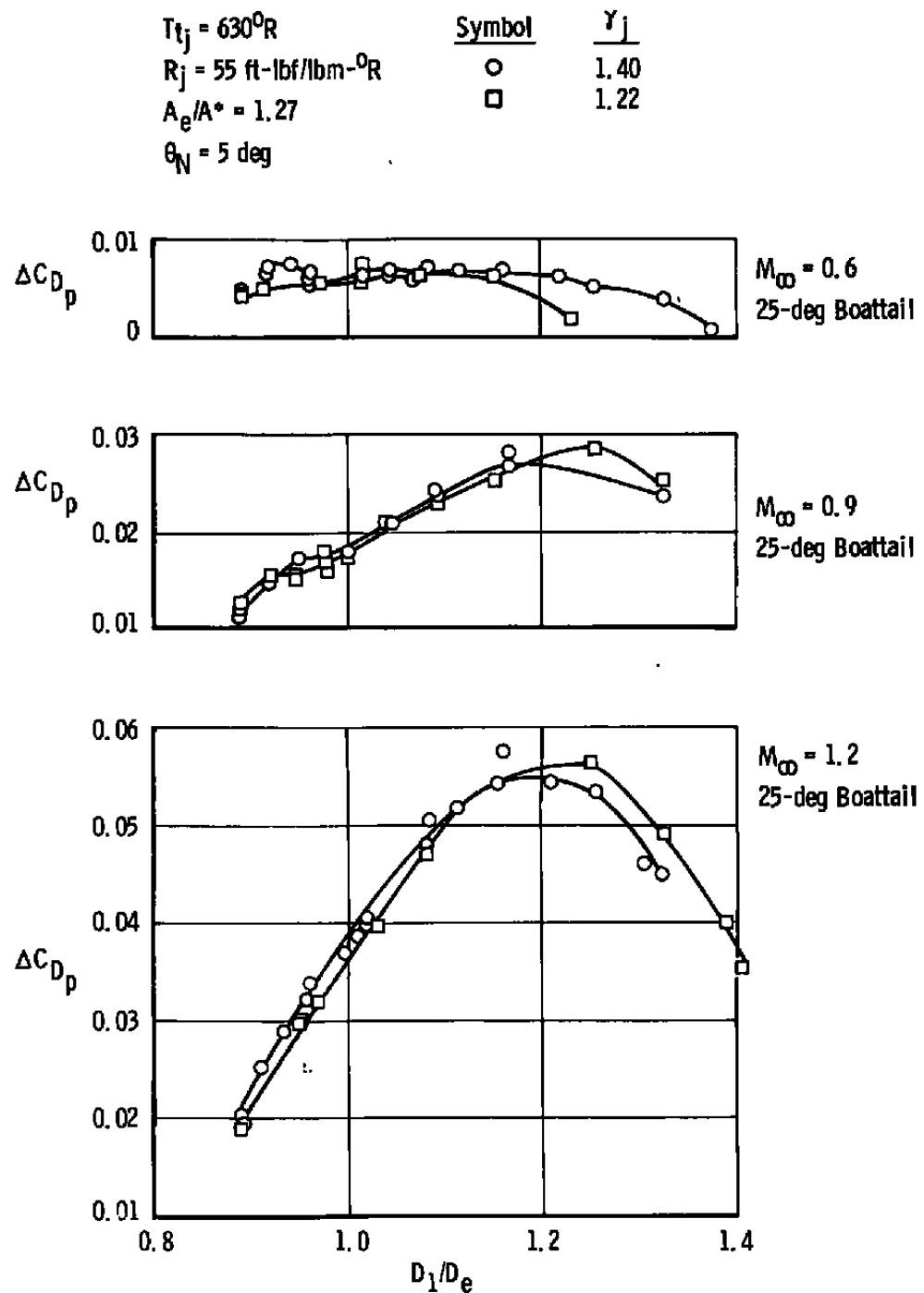
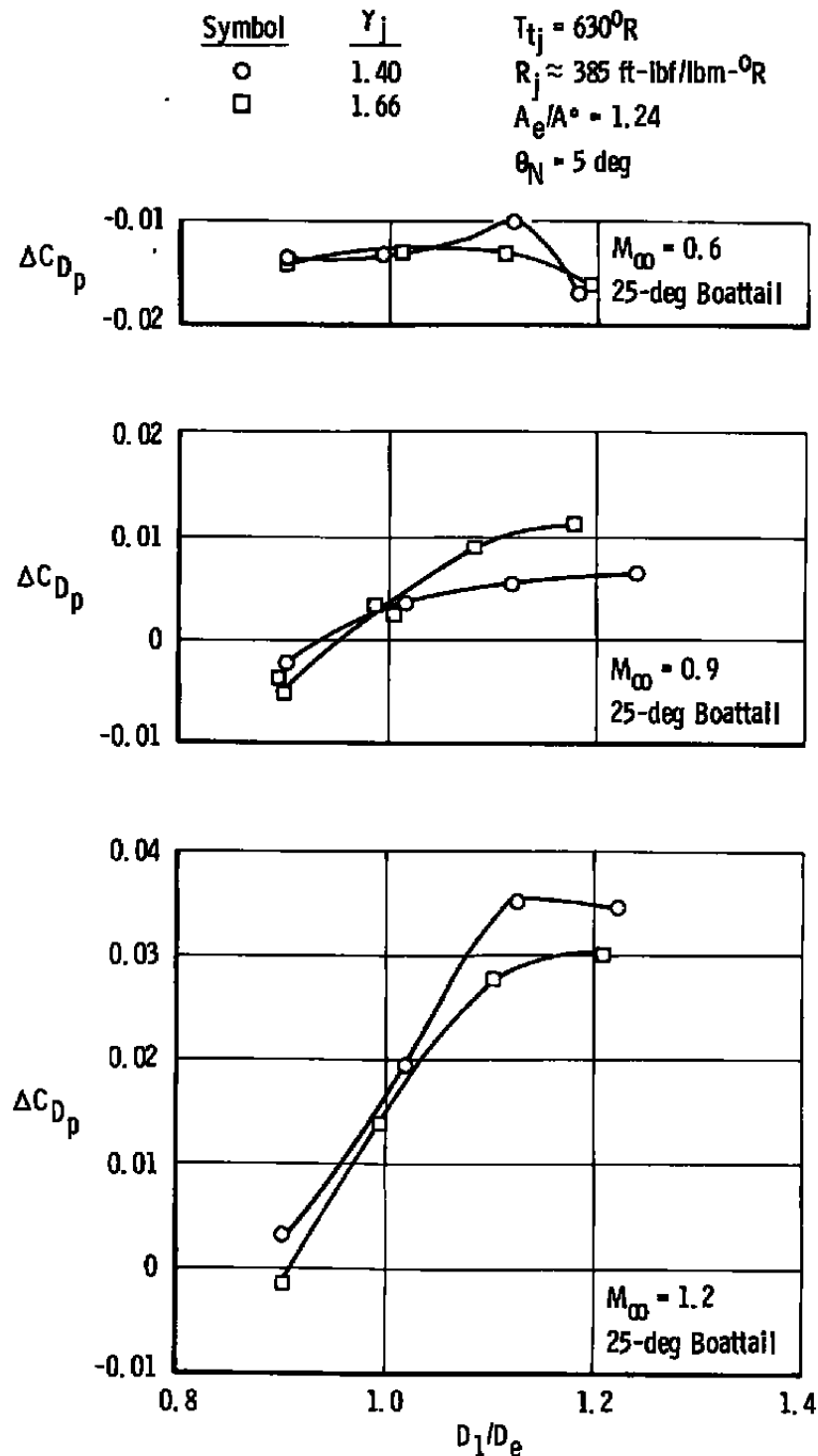


Figure 4. Gas supply system.



a. Data from Ref. 3, $R_j = 55 \text{ ft-lbf/lbm-}^{\circ}\text{R}$
Figure 5. Jet specific heat ratio effects on afterbody drag coefficient increment.



b. Data from current experiments, $R_j = 385 \text{ ft-lbf/lbm-}^{\circ}\text{R}$
 Figure 5. Concluded.

Symbol	A_e/A^*	θ_N , deg	$T_{tj} = 630^0R$
○	1.00	0	$\gamma_j = 1.40$
□	1.24	5	$R_j = 55 \text{ ft-lbf/lbm}^{-0.8}R$
△	2.96	5	

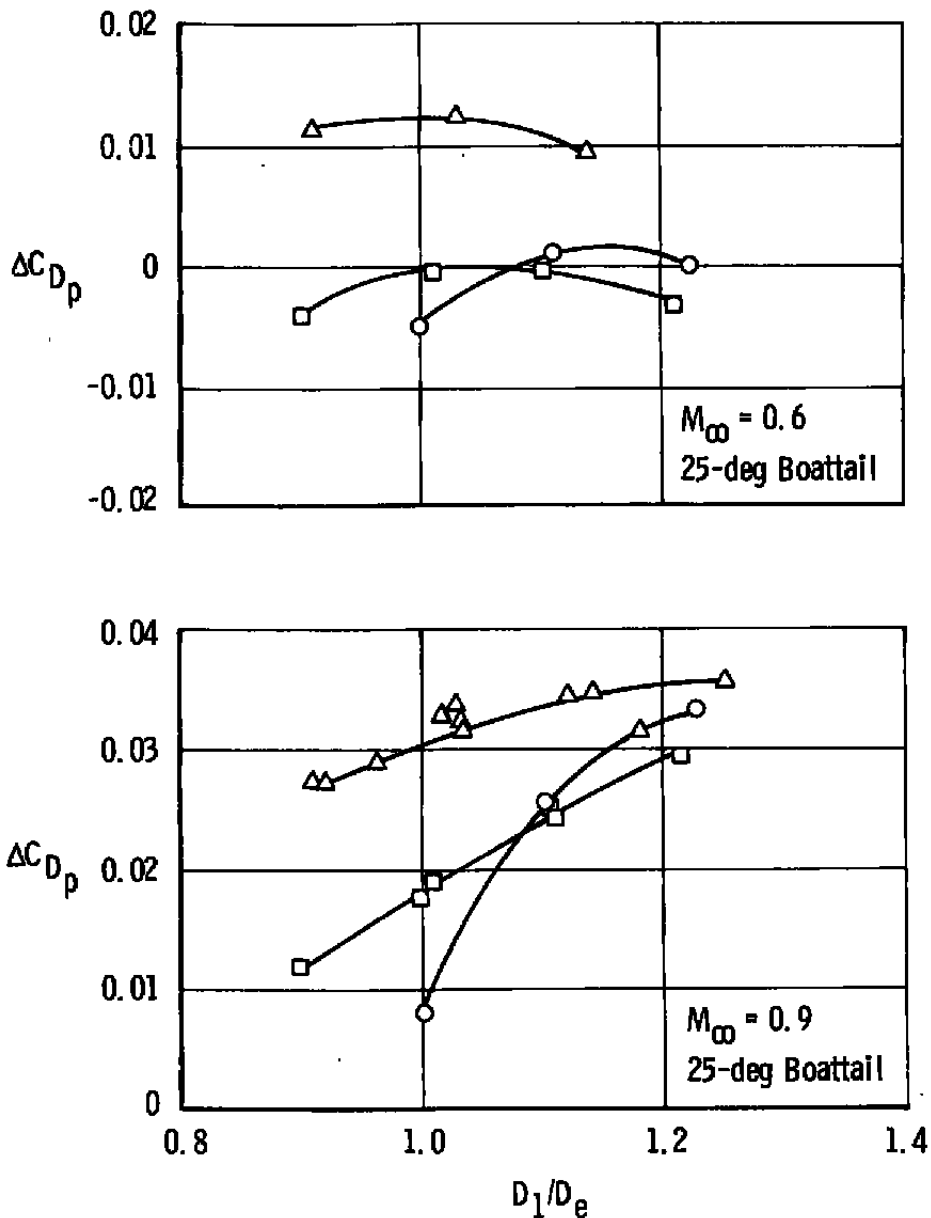


Figure 6. Nozzle area ratio effects on afterbody drag coefficient increment.

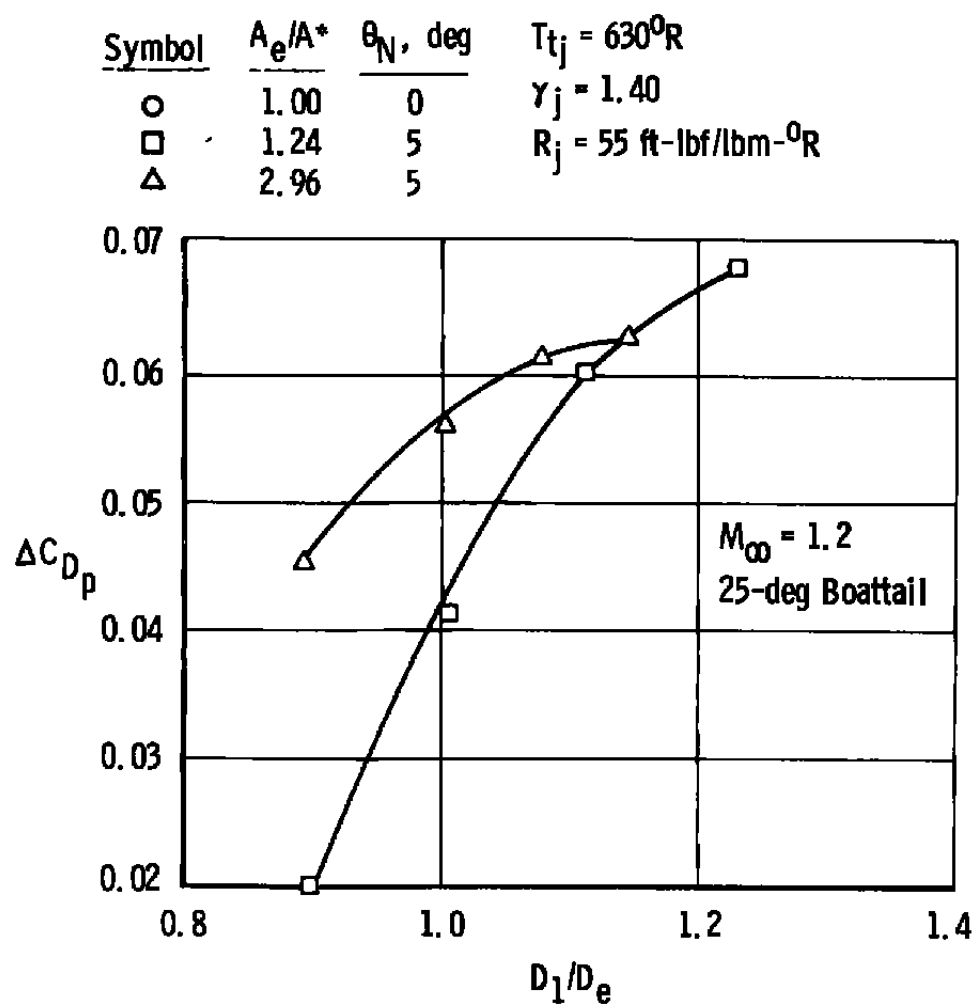


Figure 6. Concluded.

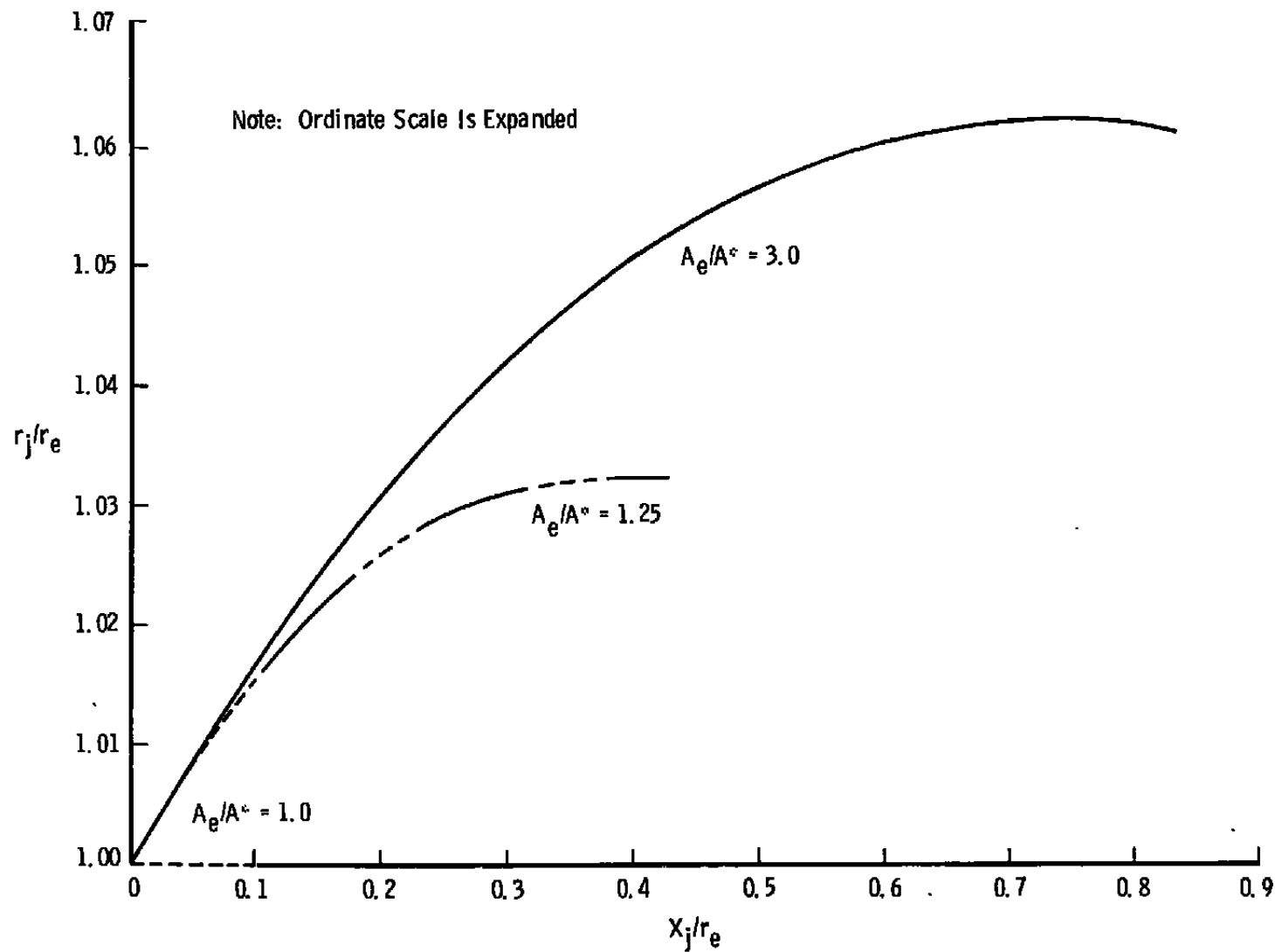
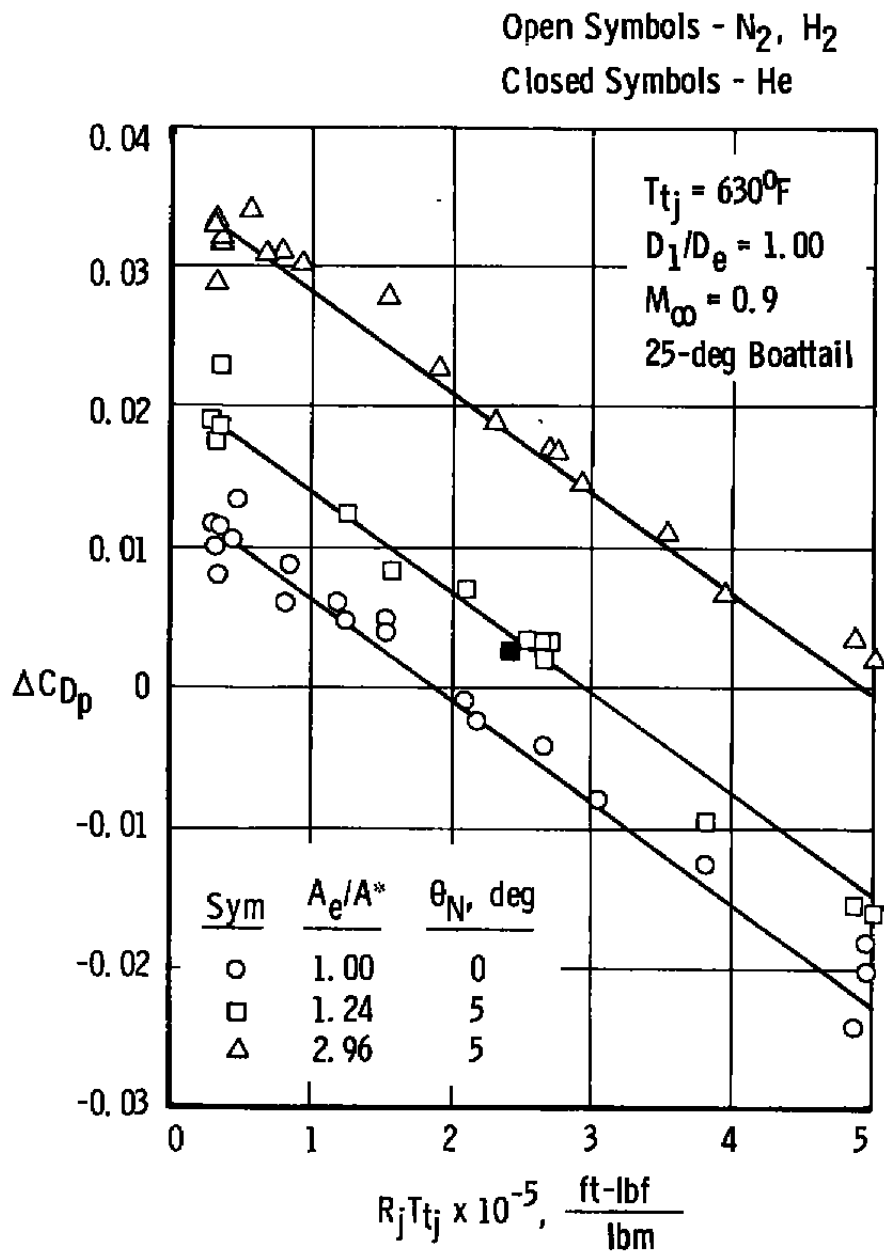
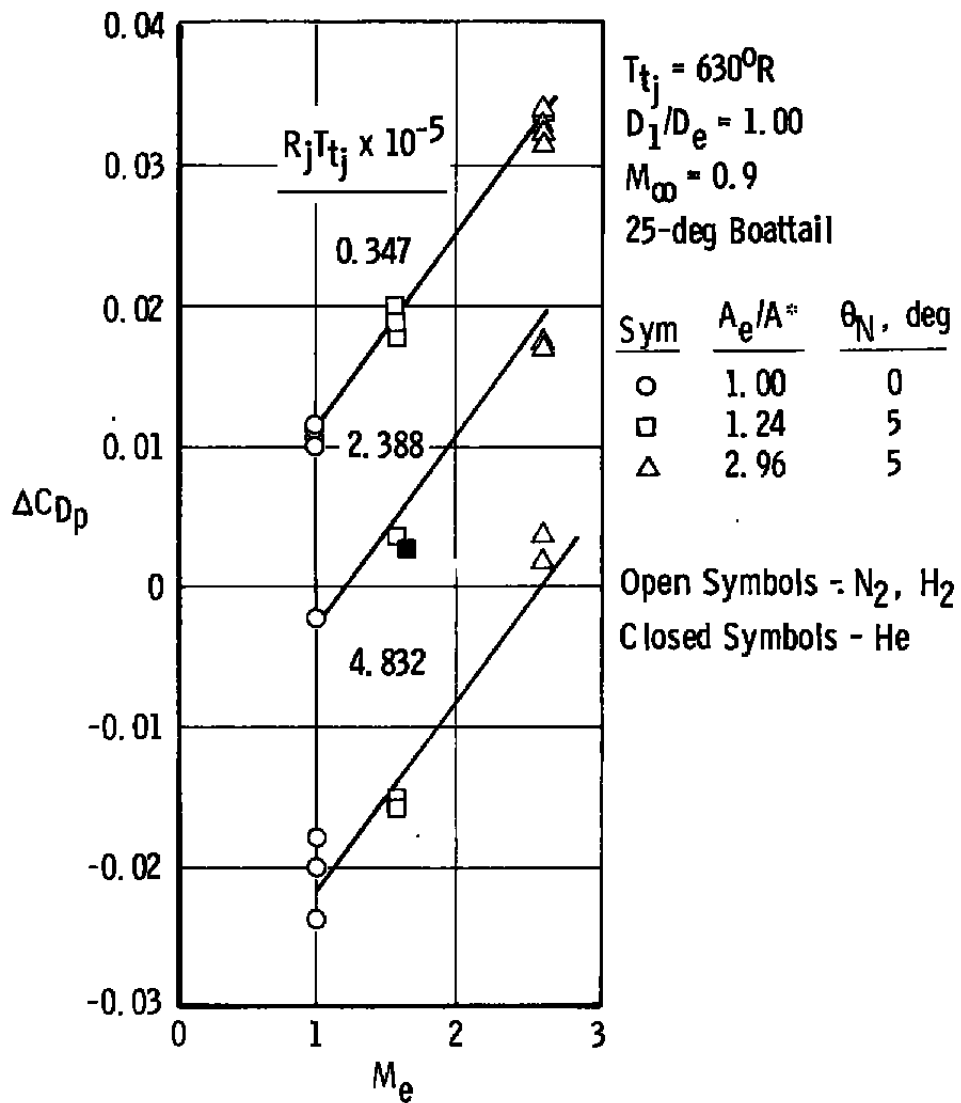


Figure 7. Effect of nozzle area ratio on jet plume boundaries
at nozzle design pressure ratio ($D_1/D_e = 1.0$).

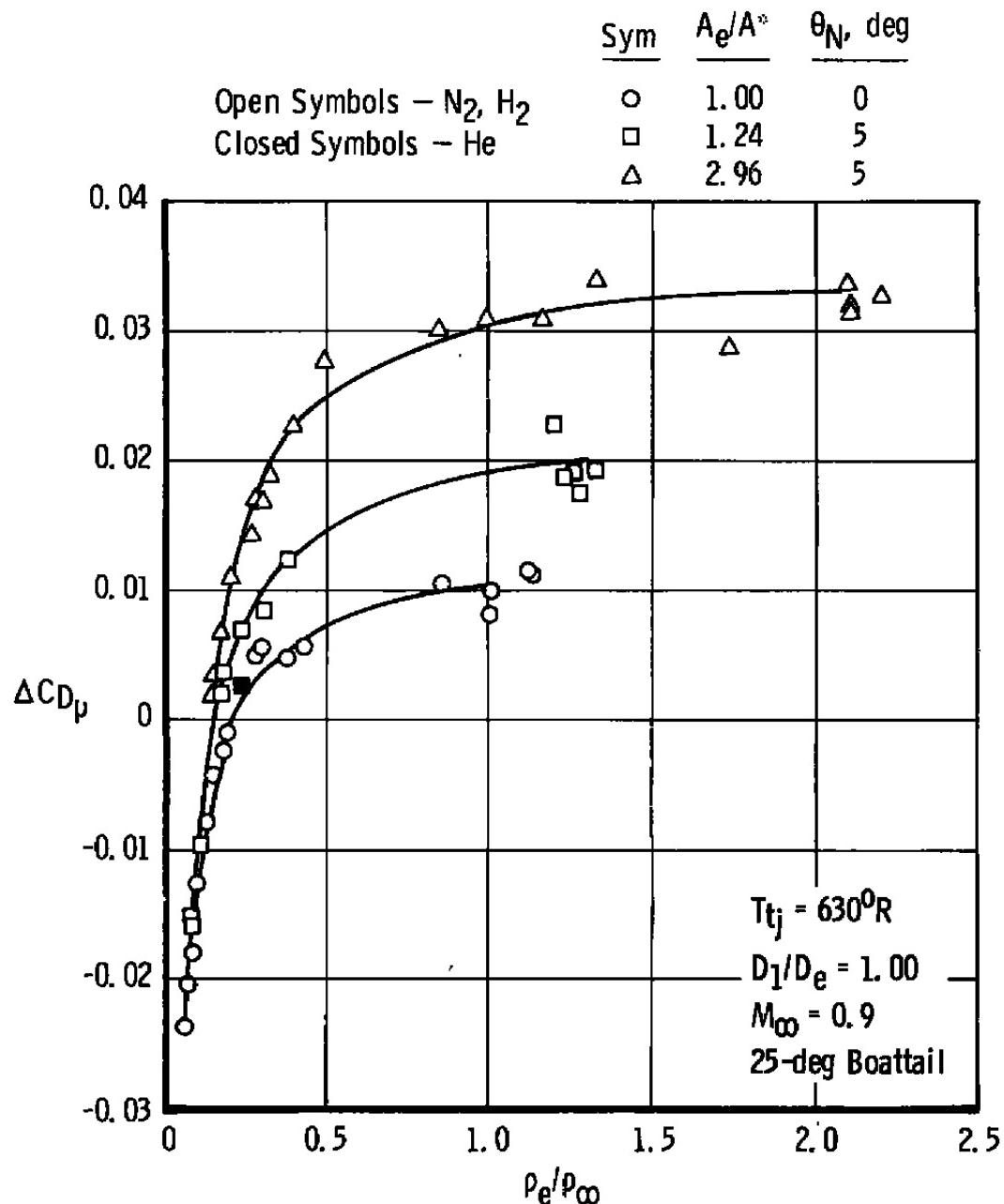


a. Product of jet gas constant and jet temperature

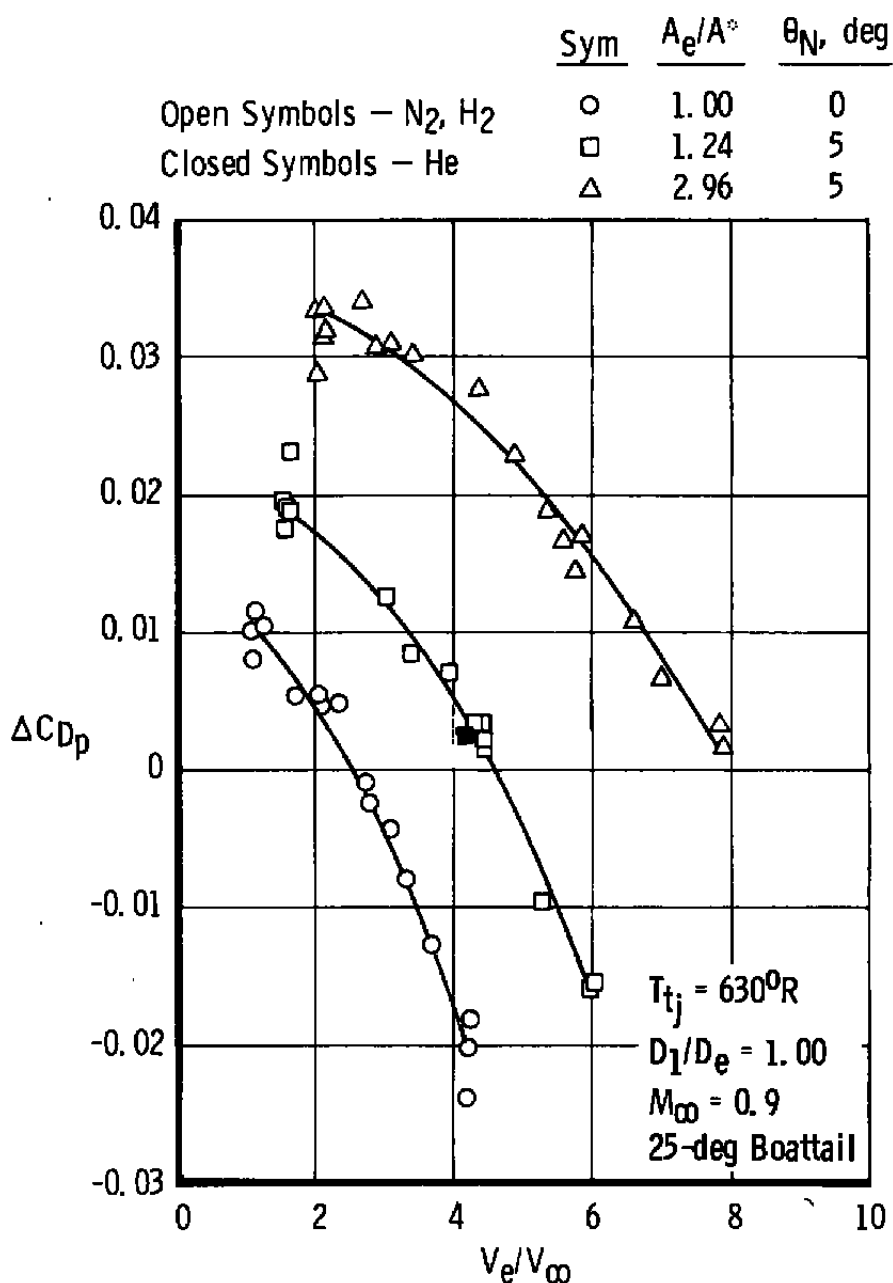
Figure 8. Jet mixing effects on afterbody drag coefficient increment produced by variations in jet molecular weight and nozzle area ratio.



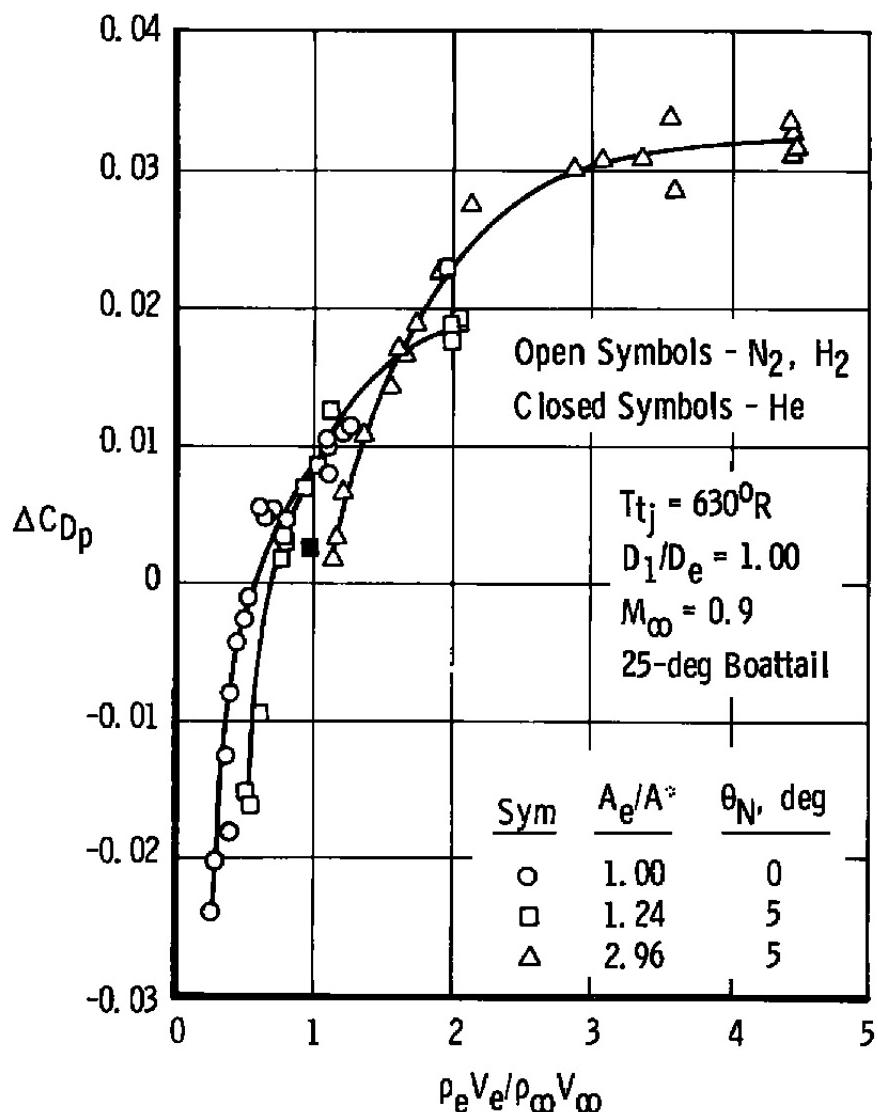
b. Jet exit Mach number
Figure 8. Continued.



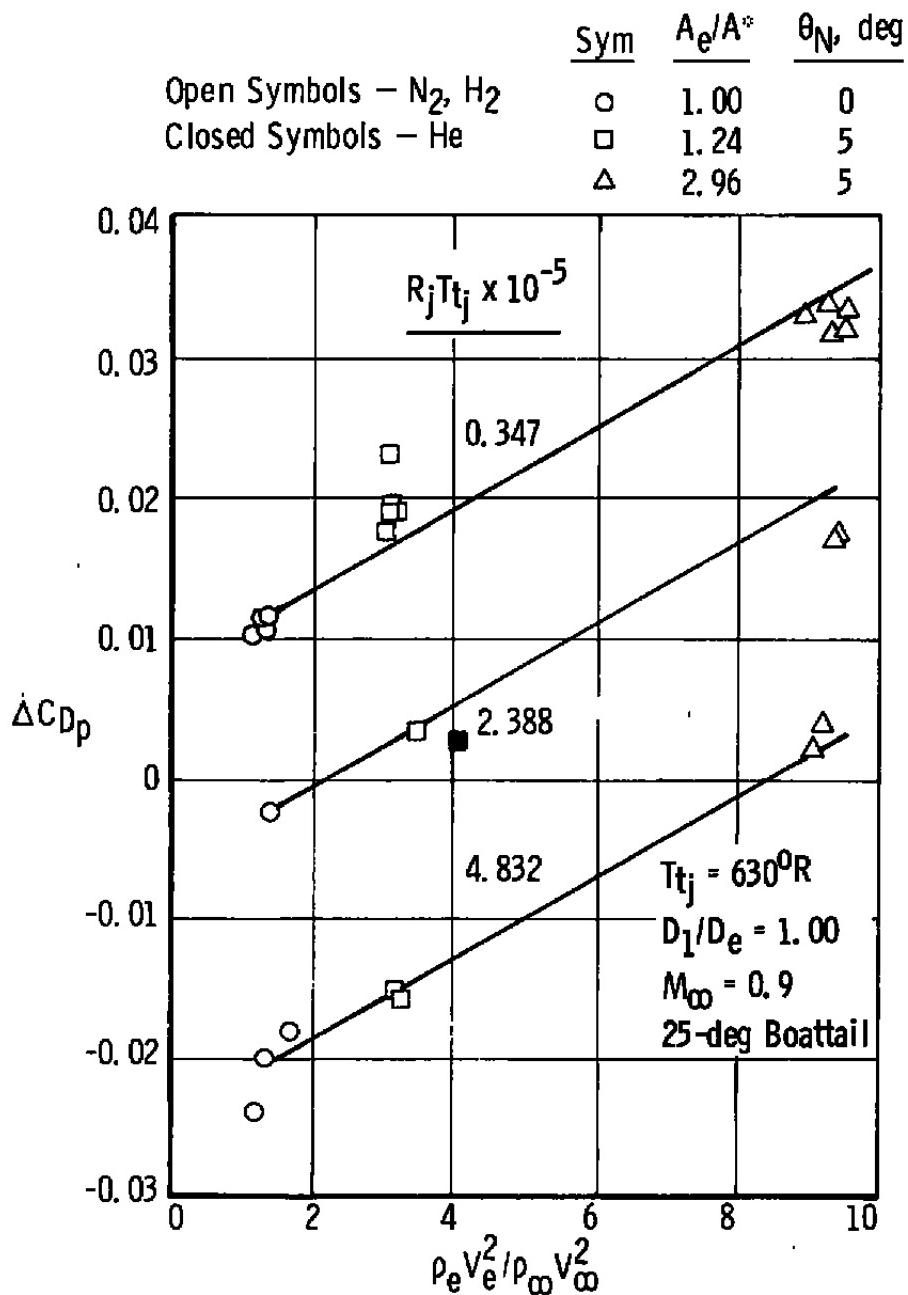
c. Jet-to-free-stream density ratio
 Figure 8. Continued.



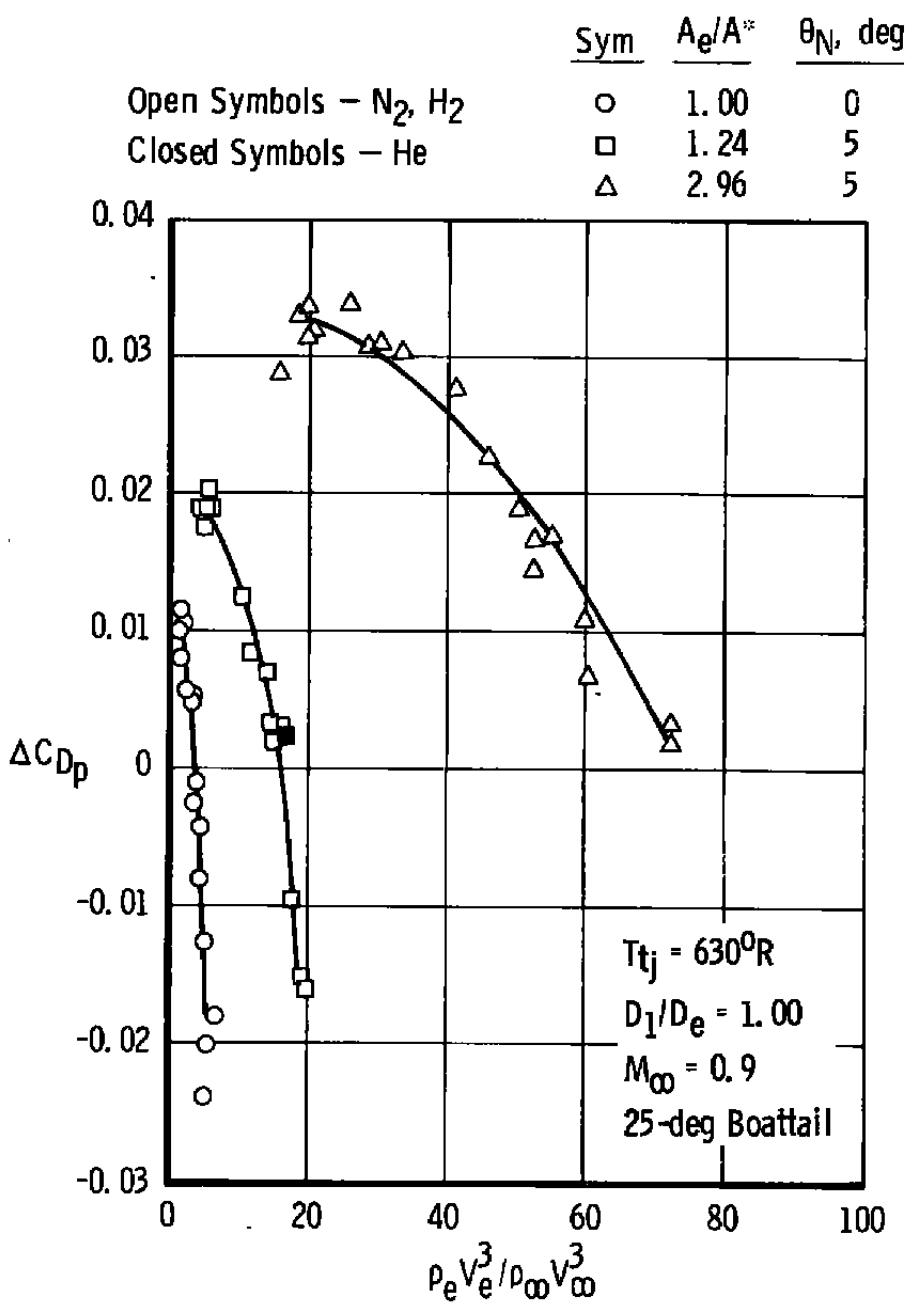
d. Jet-to-free-stream velocity ratio
Figure 8. Continued.



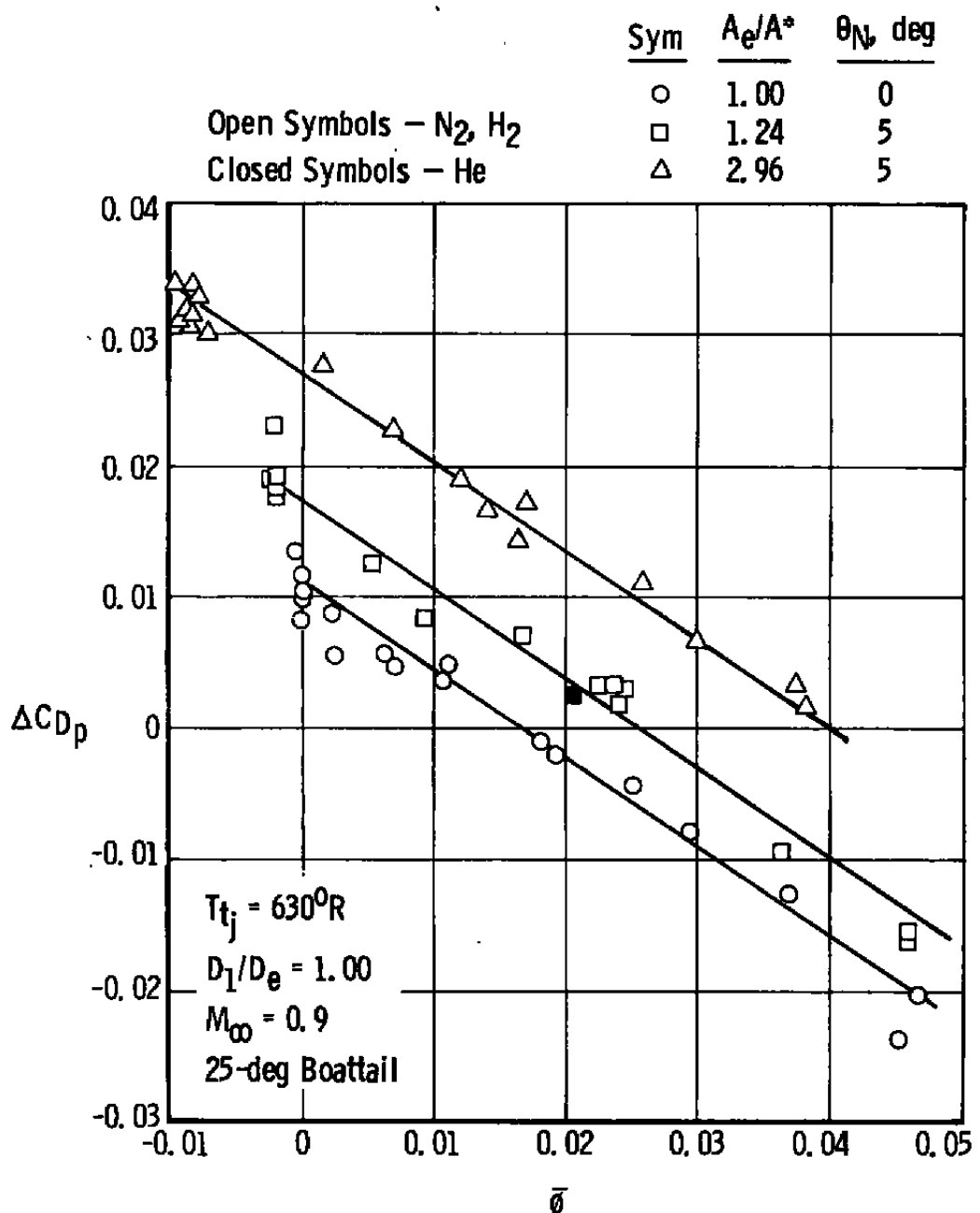
e. Jet-to-free-stream mass flux ratio
Figure 8. Continued.



f. Jet-to-free-stream momentum flux ratio
 Figure 8. Continued.



g. Jet-to-free-stream kinetic energy flux ratio
 Figure 8. Continued.



h. Induced jet-to-free-stream velocity ratio
 Figure 8. Concluded.

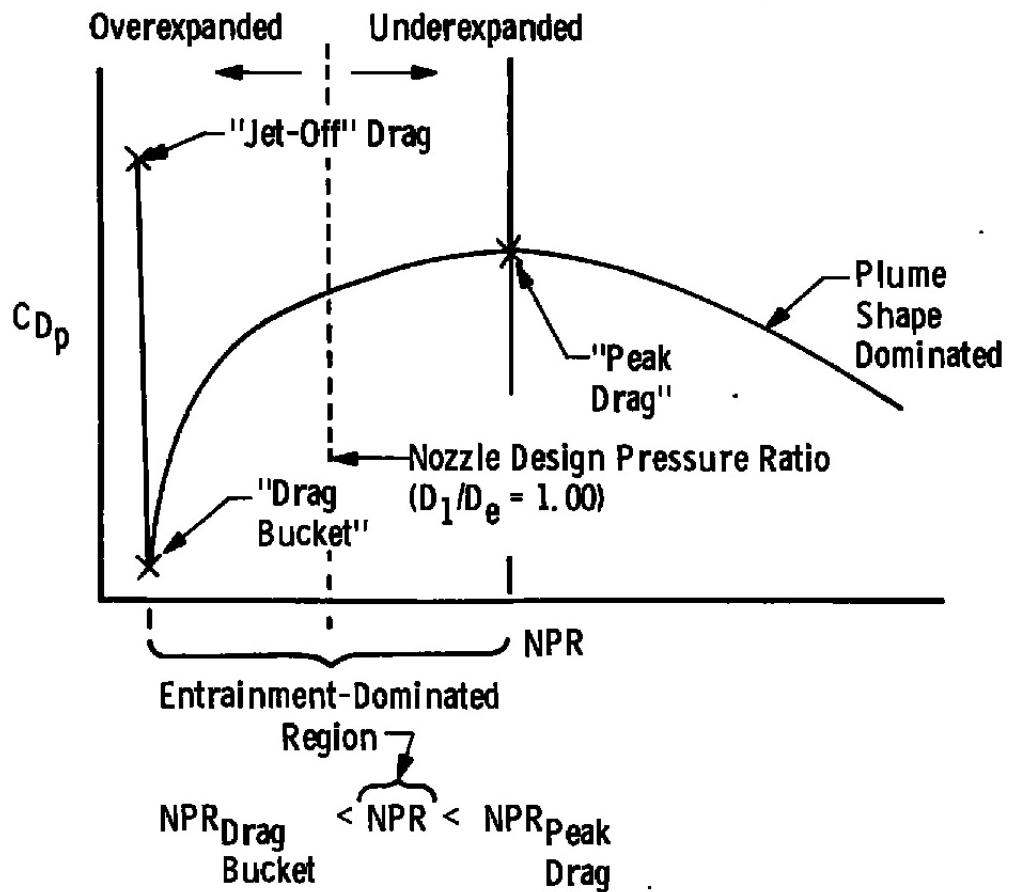


Figure 9. Typical variation of afterbody drag coefficient with nozzle pressure ratio.

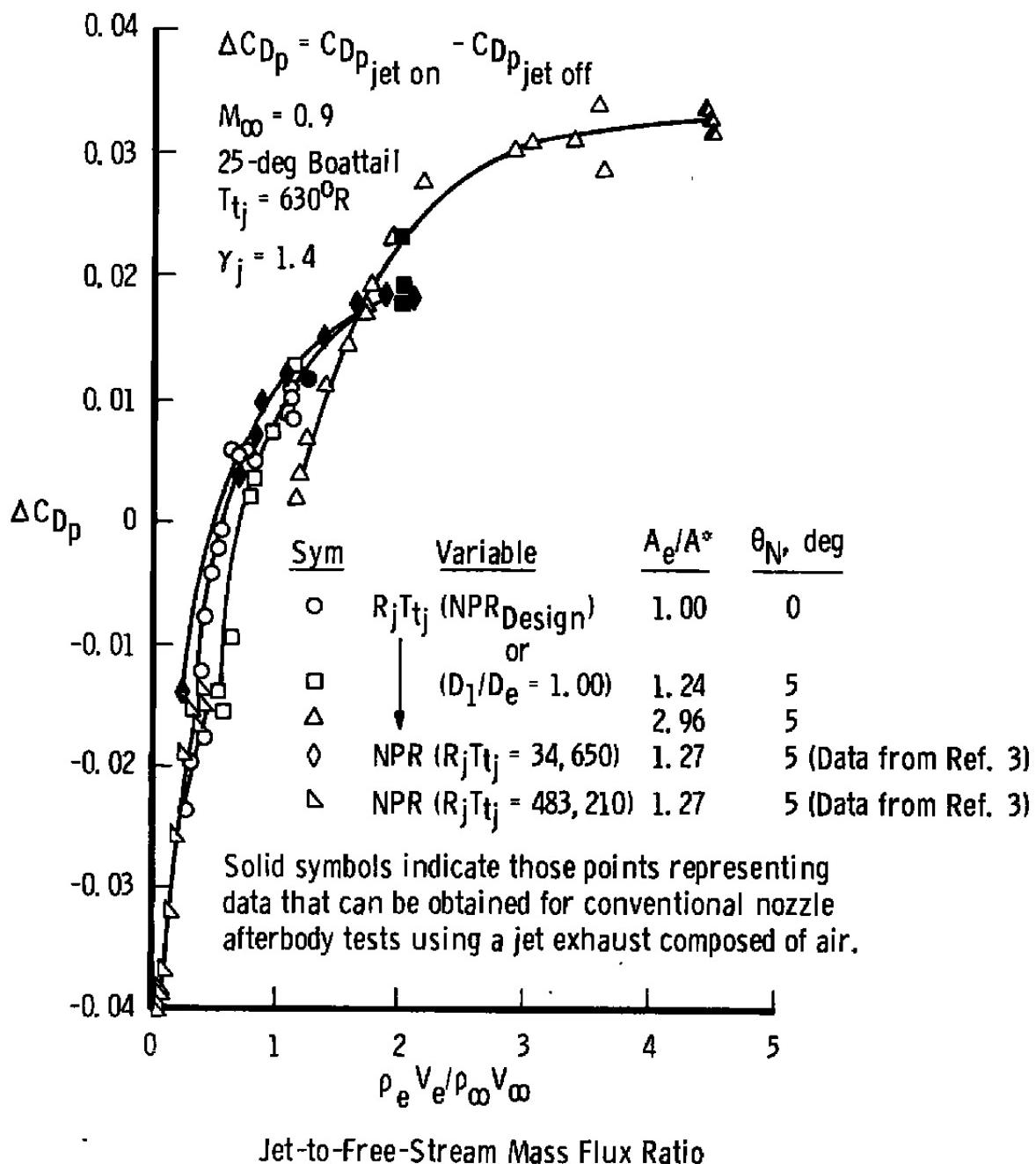


Figure 10. Comparison of jet mixing effects on afterbody drag coefficient increment produced by variations in jet molecular weight, nozzle area ratio, and nozzle pressure ratio at overexpanded jet conditions.

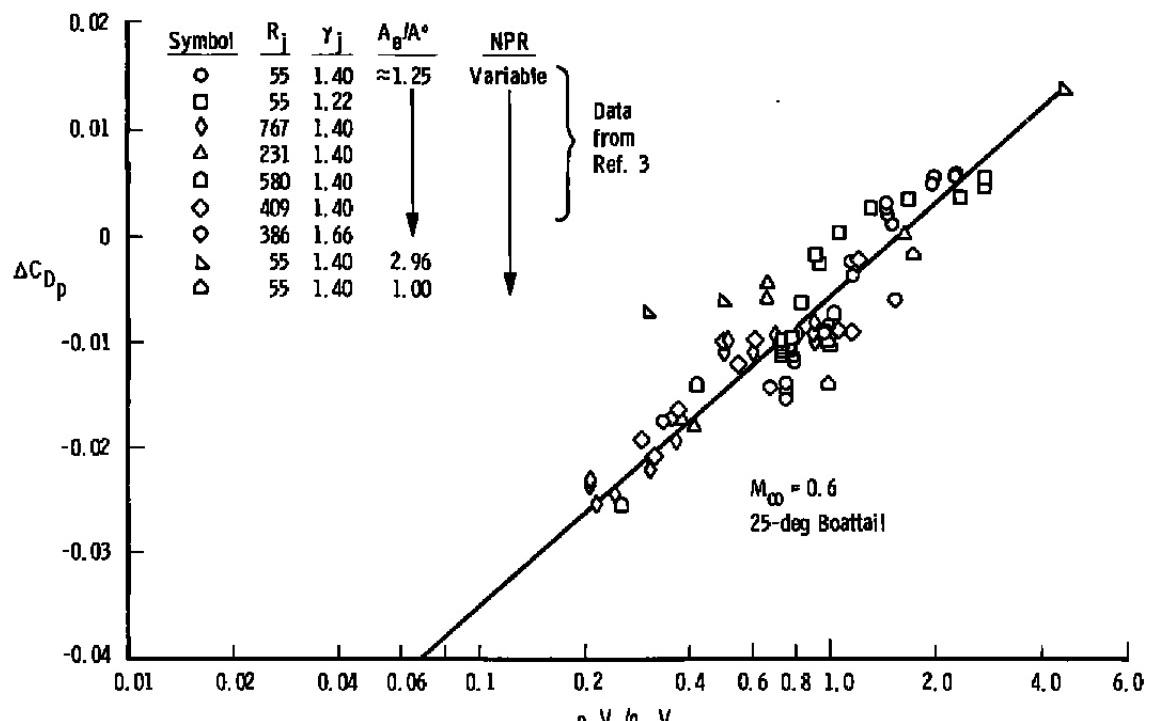
a. $M_\infty = 0.6$

Figure 11. Correlation of jet mixing effects on afterbody pressure drag coefficient increment as a logarithmic function of jet-to-free-stream mass flux ratio.

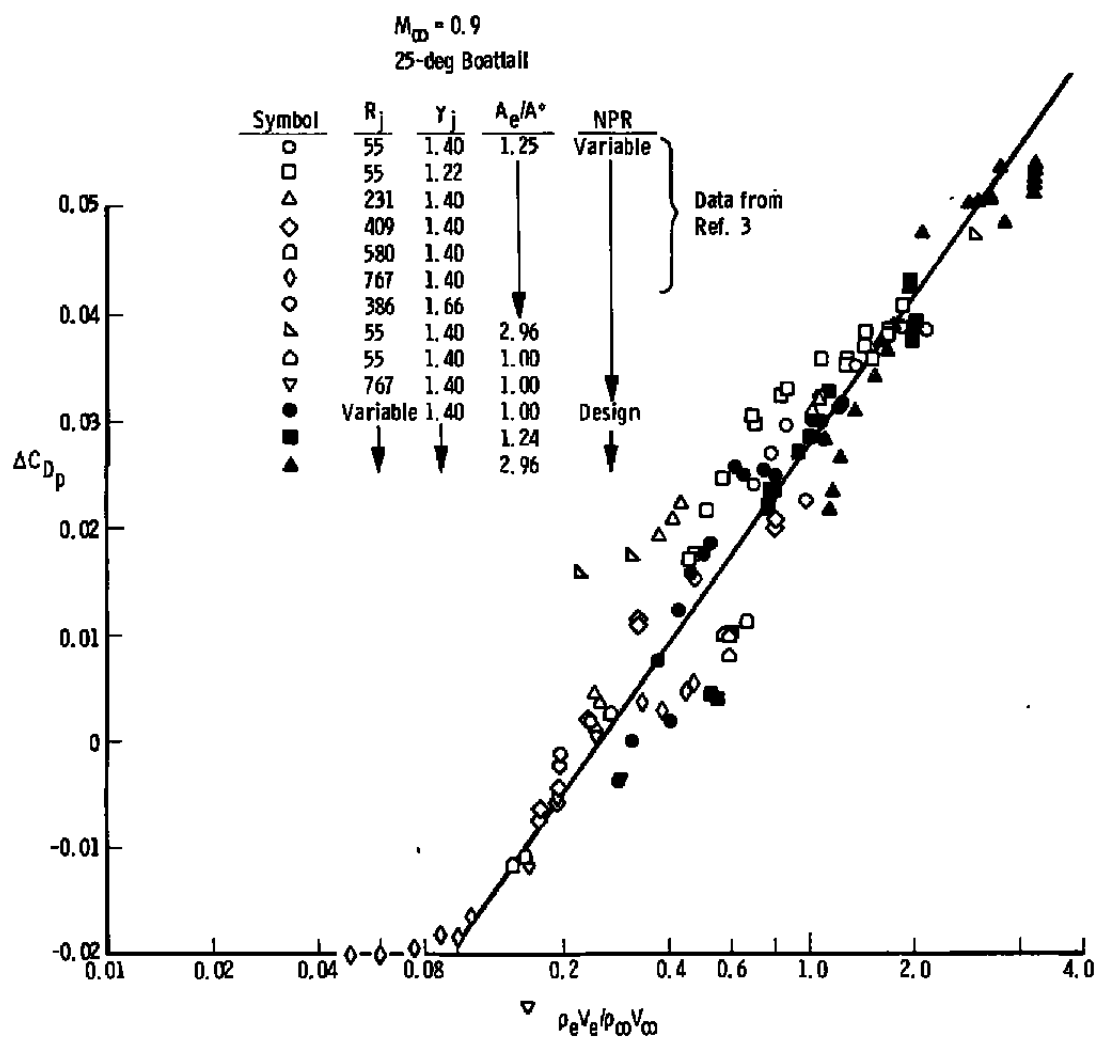
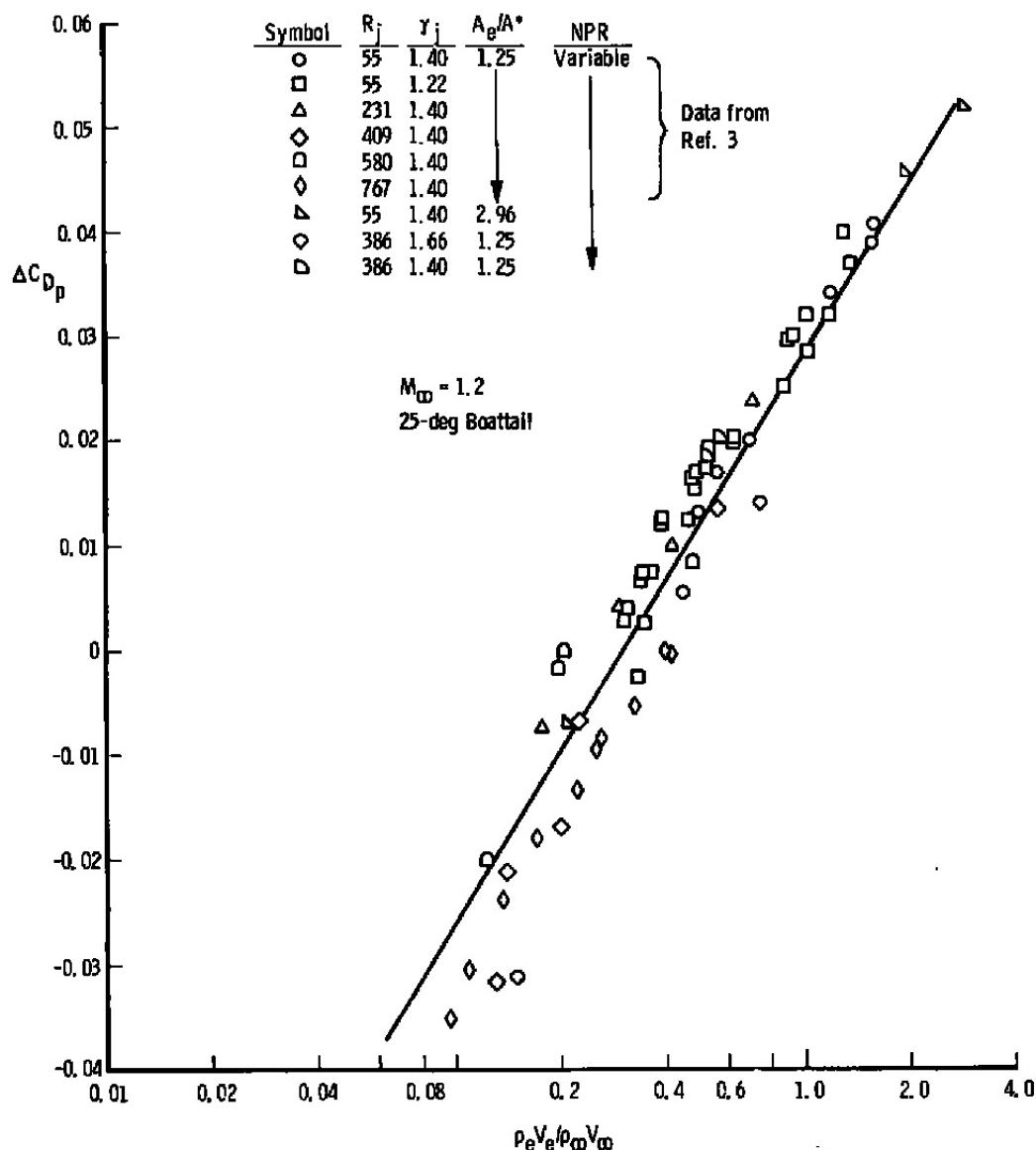


Figure 11. Continued.



c. $M_\infty = 1.2$
Figure 11. Concluded.

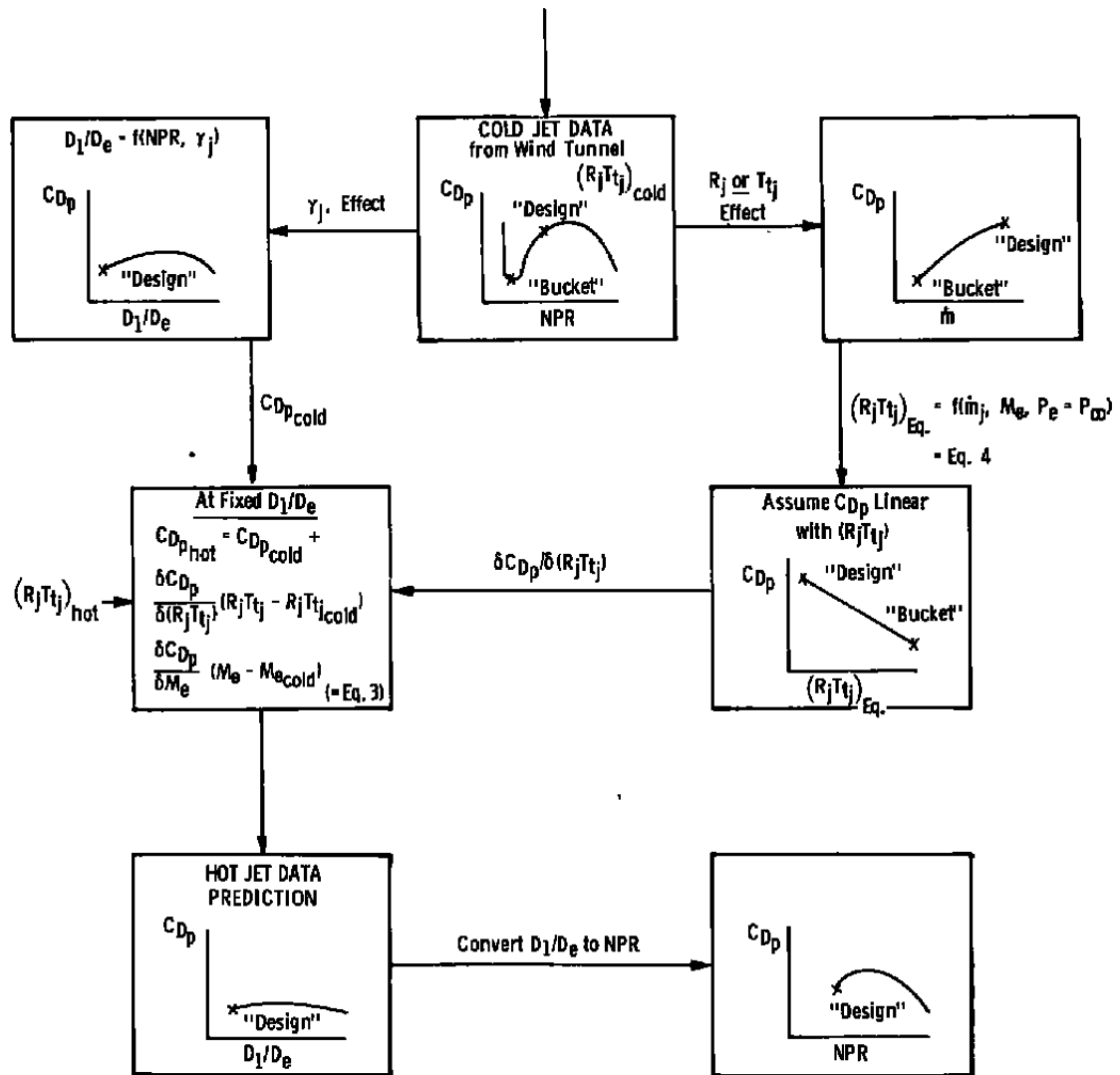
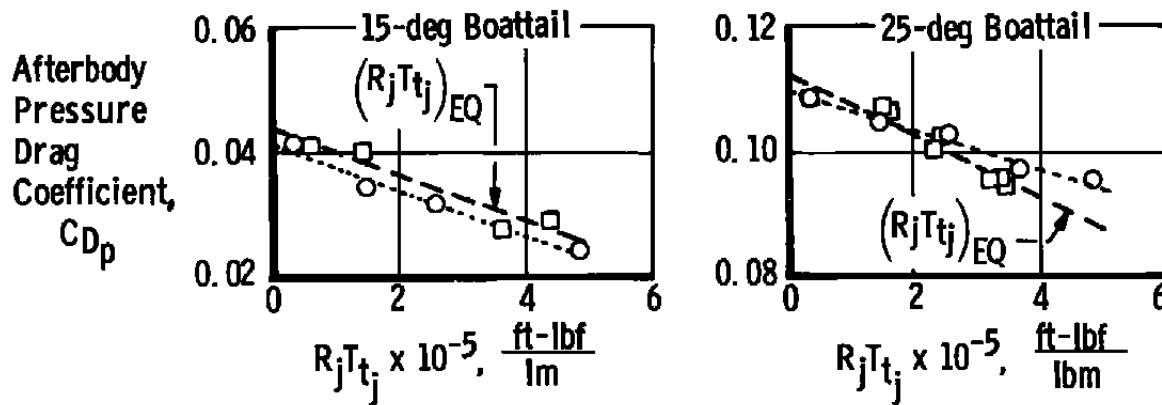


Figure 12. Proposed method for correcting afterbody drag for jet temperature effects.

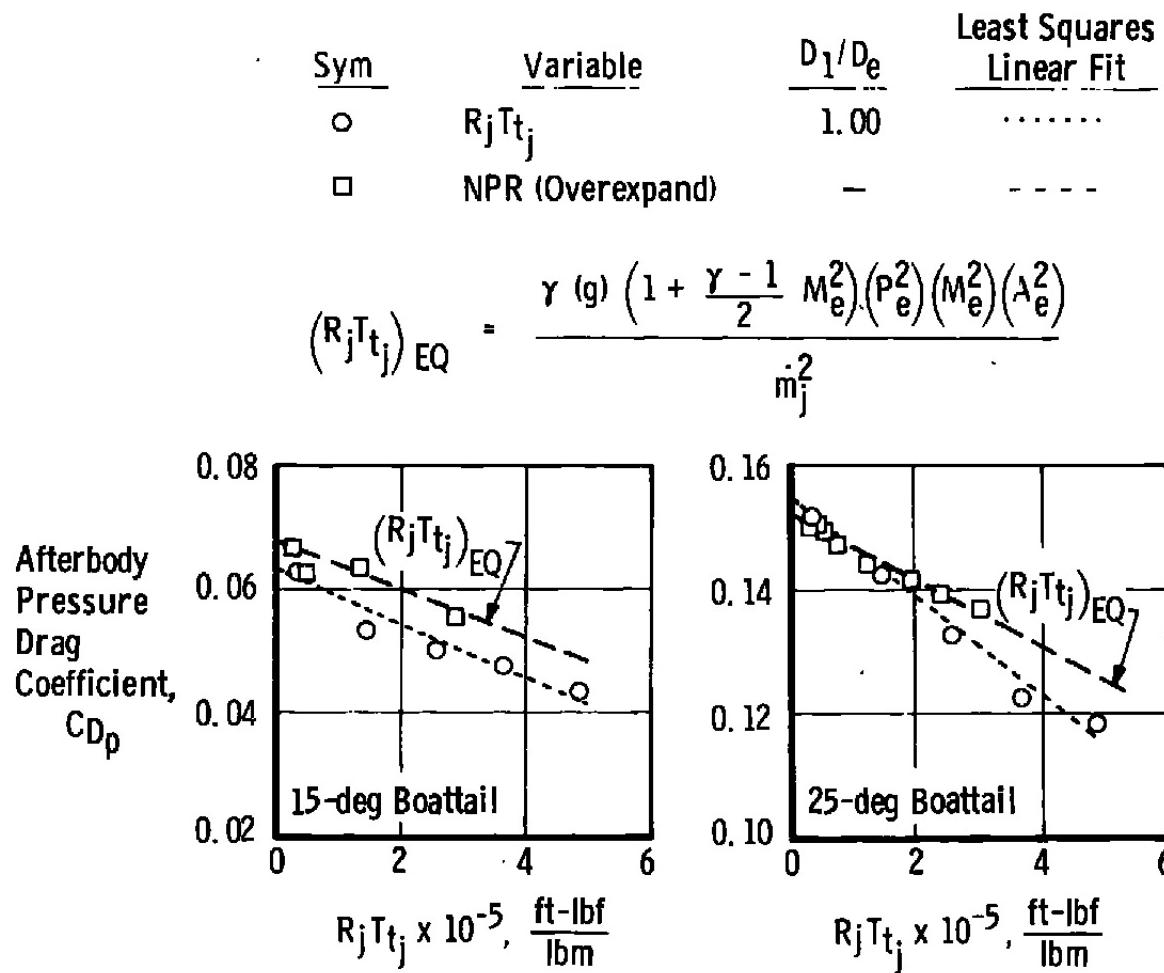
<u>Sym</u>	<u>Variable</u>	D_1/D_e	Least Squares Linear Fit
○	$R_j T_{tj}$	1.00
□	NPR (Overexpand)	—	- - -

$$(R_j T_{tj})_{EQ} = \frac{\gamma(g) \left(1 + \frac{\gamma - 1}{2} M_e^2\right) (P_e^2) (M_e^2) (A_e^2)}{m_j^2}$$



a. $M_\infty = 0.6$

Figure 13. Comparisons of actual and estimated drag coefficient sensitivity to the $R_j T_{tj}$ product.



b. $M_\infty = 0.9$
Figure 13. Continued.

Sym	Variable	D_1/D_e	Least Squares Linear Fit
○	$R_j T_{tj}$	1.00	-----
□'	NPR (Overexpand)	—	— — —

$$(R_j T_{tj})_{EQ} = \frac{\gamma (g) \left(1 + \frac{\gamma - 1}{2} M_e^2 \right) (P_e^2) (M_e^2) (A_e^2)}{m_j^2}$$

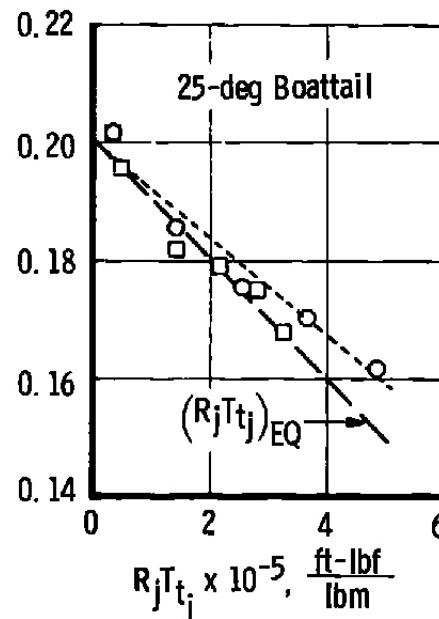
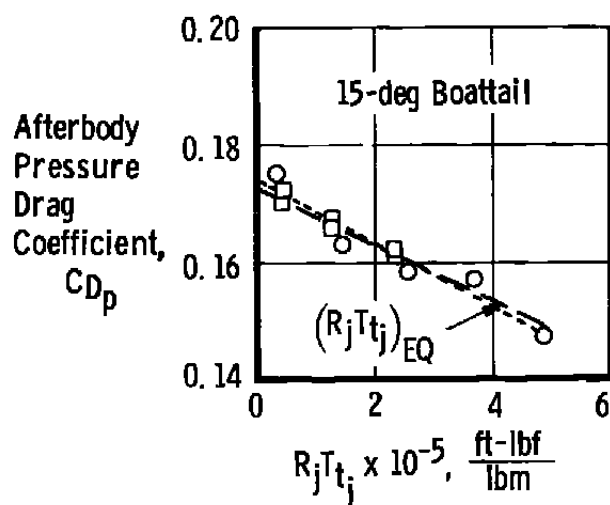
c. $M_\infty = 1.2$

Figure 13. Concluded.

Table 1. External Pressure Orifice Locations
a. Afterbody Pressures

25-deg Boattail		
X, in.	Y, in.	ϕ , deg
1.040	0.491	350
1.071	0.483	330
1.091	0.475	310
1.107	0.468	290
1.123	0.461	270
1.139	0.453	250
1.155	0.445	230
1.187	0.429	190
1.204	0.420	170
1.221	0.411	150
1.273	0.384	90
1.293	0.374	70
1.334	0.354	30
1.356	0.341	10
1.378	0.334	340
1.402	0.323	320
1.505	0.275	240
1.534	0.262	220
1.597	0.232	100

b. Base Pressures

25-deg Boattail		
X, in.	Y, in.	ϕ , deg
1.650		0
1.650		60
1.650		180

X = distance aft of M.S. 13.047

Y = distance from model centerline

L = afterbody length = 1.650 in.

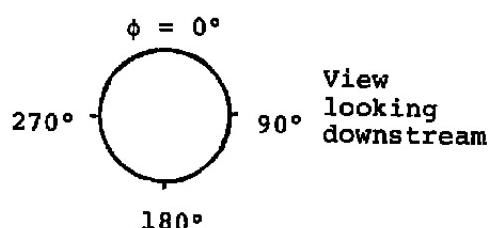


Table 2. Test Summary

Configuration Description		Variables				Mach No.		
AB/A*	θ_N DEG	GAS	R_j	γ_j	NPR	0.6	0.9	1.2
1.000	0	Jetoff	---	---	---	X	X	X
		N_2	55.16	1.40	Variable	X	X	X
		H_2	766.65	1.40	Variable	X	X	X
		Mixture N_2-H_2	Variable	1.40	≈ 1.89	X	X	X
1.240	5	Jetoff	---	---	---	X	X	X
		N_2	55.16	1.40	Variable	X	X	X
		H_2	766.65	1.40		X	X	X
		He	385.96	1.66		X	X	X
		Mixture N_2-H_2	Variable	1.40	≈ 4.18	X	X	X
		Mixture N_2-H_2	≈ 386 ≈ 409	1.40	Variable	X	X	X
2.936	5	Jetoff	---	---	---	X	X	X
		N_2	55.16	1.40	Variable	X	X	X
		H_2	766.65	1.40	Variable	X	X	X
		Mixture N_2-H_2	Variable	1.40	20.58	X	X	X

NOMENCLATURE*

A	Nozzle area, sq. in.
A_e/A*	Nozzle exit to throat area ratio
C_{Dp}	Afterbody pressure drag coefficient, $D_p/q_\infty S = -\sum(C_{p_x})(S_{p_x})/S$
C_{p_x}	Afterbody pressure coefficient, $(P_x - P_\infty)/q_\infty$
D	Nozzle diameter, in.
D_{j/D_e}	Maximum inviscid jet plume boundary diameter based on isentropic flow divided by nozzle exit diameter
D_p	Integrated afterbody pressure drag, $-\sum(p_x - p_\infty)(S_{p_x})$, lbf
g	Gravitational constant, ft/sec ²
L	Afterbody length, 1.650 in.
M	Mach number
m	Mass flow, lbm/sec
NPR	Nozzle total-to-free-stream static pressure ratio, P_t/P_∞
NSPR	Nozzle exit static-to-free-stream static pressure ratio, P_e/P_∞
P	Static pressure, psia
P_t	Total pressure, psia
q	Dynamic pressure, psi
R	Gas constant, ft-lbf/lbm-°R
RT_t	Product of gas constant and total temperature, ft-lbf/lbm
Re x 10⁻⁶	Reynolds number per foot
r	Plume boundary radius, in.
S	Maximum model cross-sectional area, 0.76 sq. in.
S_{p_x}	Projected area on afterbody assigned to C _{p_x}
T	Static temperature, °R
T_t	Total temperature, °R

*See figure at end of Nomenclature for definition of terms.

V	Velocity, ft/sec
X/L	Distance aft of model station 13.047 divided by afterbody length
x_j	Plume boundary distance aft of nozzle exit, in.
ΔC_{D_p}	Afterbody pressure drag coefficient increment, $ΔC_{D_p} = C_{D_p} - C_{D_p JETOFF}$
Δν	Incremental Prandtl-Meyer angle, $ν_1 - ν_e$, deg
γ	Ratio of specific heats
θ_N	Nozzle divergence half-angle, deg
ν	Prandtl-Meyer angle, deg
ρ	Mass density, lbm/ft ³
ρv	Mass flux, lbm/ft ² -sec
ρv²	Momentum flux, lbm/ft·sec ²
ρv³	Kinetic energy flux, lbm/sec ³
Φ	Induced jet-to-freestream velocity ratio (Ref. 10)

SUBSCRIPTS

I	Jet conditions at inviscid jet plume boundary
c	Jet conditions in nozzle plenum chamber
e	Jet conditions at nozzle exit plane
He	Helium
H₂	Hydrogen
j	Jet conditions at any given axial station
N₂	Nitrogen
v	Venturi conditions
x	Afterbody pressure tap axial location
∞	Tunnel free-stream conditions

SUPERSCRIPT

*	Jet conditions at nozzle throat
----------	---------------------------------

